Astronomy & Astrophysics manuscript no. output
July 10, 2026

The GAPS programme at TNG

LXXV. Validating and confirming Gaia sub-stellar astrometric candidates with HARPS-N

D. Barbato[1], M. Pinamonti[2], A. Sozzetti[2], S. Desidera[1], V. D'Orazi[3,1], J. Maldonado[4], K. Biazzo[5], L. Naponiello[2], A. F. Lanza[6], A. Bignamini[7], A. S. Bonomo[2], M. Brogi[2,8], L. Cabona[9], M. Damasso[2], R. Gratton[1], L. Mancini[3,2,10], G. Mantovan[12,1], D. Nardiello[11,1], M. Rainer[9], G. Guilluy[2], P. Giacobbe[2], L. Malavolta[1,11], R. Cosentino[13], W. Boschin[13,14,15], and R. Claudi[1,16]

(Affiliations can be found after the references)

Received 7 October 2025 / Accepted 19 June 2026

ABSTRACT

Context. The astrometric measurements provided by the Gaia space mission represent a key advancement in the search for and characterisation of exoplanets, helping in particular to solve the mass degeneracy intrinsic to the radial velocity (RV) method. The fact that a fraction of astrophysical false positives contaminates the current catalogue of astrometric candidate solutions requires an RV follow-up to validate and confirm such candidates.

Aims. Within the Global Architecture of Planetary Systems (GAPS) programme, we observed a selected sample of 14 stars with Gaia astrometric solutions compatible with the presence of a sub-stellar companion. The immediate aim of this survey is to identify astrophysical false positives and provide the first RV validation and confirmation of the remaining candidates.

Methods. We analysed data collected with the HARPS-N spectrograph to identify stellar binary systems from the spectral cross correlation function profiles. The remaining astrometric candidates were characterised via Markov chain Monte Carlo analysis searching for the best-fit RV solution.

Results. Among the stars in our sample with astrometric candidate solutions, we identify six as originating from close binary companions mimicking the astrometric motion of distant sub-stellar companions, from which we can estimate an updated value of 43^{+13}_{-11}% for the binary contamination fraction in the Gaia DR3 catalogue of astrometric candidates. We validate and confirm the remaining eight solutions, corresponding to giant and brown dwarf companions with minimum masses between 8 and 62 $M_{\rm Jup}$ and semi-major axes between 0.76 and 1.42 au, providing the first RV characterisation for six of these candidates and updated orbital solutions for two previously confirmed ones.

Key words. techniques: radial velocities – astrometry – planetary systems – planets and satellites: detection – brown dwarfs

1. Introduction

A key issue in current exoplanetology is the determination of the occurrence rate of systems in which companion mass tends to increase with orbital separation. Such so-called ordered systems (Mishra et al. 2023) are of special interest in the investigation of the origin of the observed variety of system architectures, with theoretical models advocating various possible formation pathways and occurrence rates. Current models argue for a weak (e.g. Schlecker et al. 2021), positive (e.g. Bitsch & Izidoro 2023), or negative (e.g. Izidoro et al. 2015 and Morbidelli et al. 2015) effect of the presence of cold Jupiters ($a > 1$ au, $0.3 < M < 20\,M_{\rm Jup}$) on the formation and evolution of inner super-Earths ($2 < M < 10\,M_\oplus$) and Neptunes ($10 < M < 20\,M_\oplus$).

Over the years, many observational campaigns have attempted to measure the occurrence rates of such ordered systems and investigate their origins. Some works find strong positive correlations between outer giants and inner low-mass exoplanets (Zhu & Wu 2018, Bryan et al. 2019, Bryan & Lee 2024, Lefèvre-Forján & Mulders 2025 and Bonomo et al. 2025), while others report a weak correlation (Rosenthal et al. 2022), no correlation (Bonomo et al. 2023), or a negative correlation (Barbato et al. 2018). Although a significant part of such a tension between observational results arises from non-trivial comparisons among different definitions of planetary categories, system multiplicity, and stellar properties in the analysed samples, another fundamental issue arises from the fact that the vast majority of intermediate-separation ($1 < a < 5$ au) cold Jupiters has been detected by radial velocity (RV) observations alone and are therefore only characterised by its minimum mass $M \sin i$. Additionally, many studies focused on determining the occurrence rate of low-mass companions in the presence of cold Jupiters (e.g. Bryan et al. 2019 and Rosenthal et al. 2022) often infer the outer companion presence from long-term RV trends, which are intrinsically degenerate with mass and separation. Therefore, RV-only studies of the demography of ordered systems suffer from the limitations imposed by the incomplete characterisation of the outer companions' orbital characteristics and true dynamical mass.

Similarly, the true mass of brown dwarfs (BD) represents a key input for formation and evolution models for these companions. While BDs are generally thought to be formed via gravitational instability (Chabrier et al. 2014 and Whitworth 2018), significant work is still needed to investigate the origin of the observed scarcity of BDs on close orbits around solar-type stars (the so-called BD desert), with different evolution pathways being proposed (Armitage & Bonnell 2002, Jumper & Fisher 2013, Ma & Ge 2014, Maldonado & Villaver 2017). Solving this issue requires large statistics and reliable true mass measurements, and as such RV-only exploration of the BD population suffers from the same limitations discussed for giant exoplanets.

Article published by EDP Sciences, to be cited as https://doi.org/10.1051/0004-6361/202557585

The ESA's Gaia space astrometry mission (Gaia Collaboration et al. 2016) represents an essential turning point, having the potential to detect thousands of cold Jupiters and BDs as distant as 5 au from their host stars (Casertano et al. 2008, Sozzetti et al. 2014, Perryman et al. 2014). Furthermore, the high-precision proper motion measurements provided by Gaia have enabled the analysis of proper motion anomaly (PMa) between the Hipparcos and Gaia epochs (e.g. Brandt 2021 and Kervella et al. 2022). The third Gaia Data Release (Gaia DR3, Gaia Collaboration et al. 2023b) produced a catalogue of 169227 non-single stars (NSS) for which the observed astrometric motion solution is consistent with a Keplerian orbit produced by an unseen massive companion. Of particular interest amongst these are ~2000 orbits consistent with companions having estimated true dynamical masses in the giant planet and BD regime. These candidates represent a fertile ground for follow-up observations resulting in the validation and characterisation of cold Jupiters such as HIP 66074 b (Gaia-3 b, Winn 2022, Marcussen & Albrecht 2023 and Sozzetti et al. 2023), Gaia-4 b (Stefánsson et al. 2025), and BDs such as LHS 1610 b (Fitzmaurice et al. 2024) and Gaia-5 b (Stefánsson et al. 2025). This continuous synergy between RVs and astrometry, additionally fuelled by future Gaia DRs, is a key asset in solving RV mass degeneracy and will allow the firm assessment of ordered system demographics based on true masses and orbits of outer companions (see e.g. Sozzetti 2024).

While encouraging, the Gaia DR3 exoplanetary potential is still limited by the presence of astrophysical false positives. Indeed, the observed photocenter motion of a binary system can be as small as the one caused by a sub-stellar companion, which would instead contribute no flux, provided that the flux ratio of the stellar binary components is similar to their mass ratio (see e.g. Gaia Collaboration et al. 2023a and Marcussen & Albrecht 2023). As such, it is known that a portion of the small photocenter motions observed by Gaia can be caused by a stellar binary companion mimicking the astrometric motion produced by a massive sub-stellar companion. Holl et al. (2023) estimated that ~ 10% of DR3 astrometric orbital solutions consistent with sub-stellar companions may actually be caused by this binary contamination effect. Luckily, such astrophysical false positives can be recognised by RV follow-up campaigns, as high signal-to-noise ratio (S/N) spectra can identify double-lined spectroscopic binaries (SB2). Indeed, the RV follow-up campaign of 28 NSS candidates detailed in Stefánsson et al. (2025) results in an updated estimate of binary contamination of ~32%, a value notably larger than the one derived in Holl et al. (2023). As such, RV follow-up campaigns of a promising Gaia NSS compatible with planetary or BD companions represent a key asset in recognising false positives and provide an updated assessment of the binary contamination in DR3 astrometric solutions in preparation for future Gaia releases.

In this context, in October 2023 the Global Architecture of Planetary Systems (GAPS, see Covino et al. 2013 and Desidera et al. 2013) collaboration[1] started an intense RV observational campaign of 35 stars orbited by known or confirmed cold Jupiters and low-mass BDs using the High Accuracy Radial velocity Planet Searcher in the Northern hemisphere (HARPS-N; see Cosentino et al. 2012) spectrograph mounted on the Telescopio Nazionale Galileo (TNG) in La Palma. Of these outer companions, 21 have true masses and full orbits measured based on the combination of literature RVs, PMa, and Gaia DR3 astrometric orbital solutions, while the remaining 14 are Gaia NSS candidates in need of validation through RV follow-up observations lacking any public RV data at the moment of their inclusion in our sample. These 14 targets were selected from the NSS catalogue by virtue of their distance (<200 pc), brightness (G <12 mag), declination ($\delta > -10$ deg), and available astrometric candidate solutions compatible with an estimated true-companion mass <65 $M_{\rm Jup}$ and orbital separation between 1 and 2 au. The aim of this ongoing observational campaign is threefold: identify astrophysical false positives in the selected Gaia DR3 astrometric orbital solutions; provide first RV validation of the remaining candidates; and, finally, perform a deep search for short-period super-Earths and Neptunes in the presence of known massive outer companions to directly measure the occurrence rate of ordered systems.

In this paper we present the first results of this ongoing campaign, focusing on the refutation and validation of 14 Gaia NSS astrometric candidates, while additional noteworthy results from this campaign will be presented in Pinamonti et al. (2026) and other forthcoming papers. This paper is structured as follows. In Sect. 2 we provide an updated description of the physical characteristics of the stars populating the sample analysed in this work, before focusing on the identification of six astrophysical false positives contaminating the astrometric solutions in Sect. 3. In Sect. 4 we turn our attention towards the confirmation of eight astrometric solutions through the robust characterisation of full RV orbits. We finally discuss our results and the future perspectives of the ongoing Gaia follow-up survey in Sect. 5.

2. Stellar parameters

We derived spectroscopic stellar parameters for the stars in our sample using the HARPS-N spectra collected during our survey, following different procedures depending on the star spectral type. We note that this approach is not applicable to the stars we identify as SB2 (see Sect. 3) due to the intrinsic difficulties in disentangling the spectra of the two stellar components. As a result, the following spectroscopic analysis refers to the stars hosting validated companions (see Sect. 4).

For stars with spectral types up from late-K and early-M we computed basic stellar parameters (effective temperature, surface gravity, iron abundance) using a methodology developed by Maldonado et al. (2015) and based on ratios of spectral features (see also Maldonado et al. 2017). For stars with spectral types up to mid-K we instead followed the procedure described in Biazzo et al. (2022). In particular, we considered the list of iron lines by the latter authors and Dal Ponte et al. (2025) and then measured the line equivalent widths with the `ARESv2` tool (Sousa et al. 2015) and double-checked with `IRAF` (Tody 1993). We considered the `MARCS` atmospheric models (Gustafsson et al. 2008) and applied the `pyMOOGi` code (Sneden 1973 and Adamow 2017) as a spectral analysis package. We thus derived the final effective temperature, $T_{\rm eff}$; surface gravity, $\log g$; iron abundance [Fe/H]; and microturbulence velocity, $v_{\rm micro}$ (listed in Table A.2).

In order to have an updated characterisation of stellar mass, radius, density, luminosity and age we fitted the stellar spectral energy distributions (SEDs) using the MESA Isochrones and Stellar Tracks (MIST) (Dotter 2016 and Choi et al. 2016) via the `IDL` suite `EXOFASTv2` (see Eastman et al. 2019 for a detailed description of the method) considering all available archival magnitudes. We imposed Gaussian priors on the star's parallax ϖ based on the Gaia DR3 astrometric measurement, as well as on the effective temperature, $T_{\rm eff}$, and iron abundance, [Fe/H], based on their values obtained as detailed in the previous paragraph. For the stars we identify as SB2, for which the spectroscopic analysis was not possible, we based the $T_{\rm eff}$ and [Fe/H] priors on the respective

[1] https://www.gaps.inaf.it

values in the Anders et al. (2022) photo-astrometric catalogue. We neglected the effects of extinction, as most of the stars in our sample are relatively nearby (<150 pc) and are therefore not affected by significant extinction, while the most distant stars in our sample are identified as SB2 in Section 3.

We additionally computed the kinematic ages for the stars in our sample following Almeida-Fernandes & Rocha-Pinto (2018), computing the Galactic velocity vector (U, V, W) from each star's systematic RV, proper motions, and parallax. When available, we used the 25 yr average proper motions listed in the Hipparcos-Gaia Catalog of Accelerations (HGCA, see Brandt 2021), using the Gaia DR3 values for the stars not in the HGCA.

We additionally use the Python tool `ACTIN2`[2] (Gomes da Silva et al. 2018, 2021) to extract activity indicators from the collected HARPS-N spectra, considering emission from the Ca II H&K ($S_{\rm MW}$), Hα, Na I D2, and He I lines in particular. We note that no stars in our sample exhibit strong activity levels, and we analysed the activity indices' time series and their relationships with the observed RV variations for each star in Section 4.

All relevant archival stellar information, as well as the parameters resulting from the analyses detailed in this section, are listed in Table A.1 for the SB2 stars and in Table A.2 for the stars hosting Gaia candidates that we validated in this work. For the latter, we note that our derived stellar masses are compatible within 1.5σ with the adopted primary masses in the NSS catalogue, which we report for each star in Section 4. We must note, however, that the SED fit performed for the SB2s may be influenced by their binary nature and lead to less-than-robust results.

3. Binary contamination

As mentioned in Sect. 1, stellar binaries are noted to be the main source of such false positives (Gaia Collaboration et al. 2023a, Holl et al. 2023 and Marcussen & Albrecht 2023), with binary components having a mass ratio similar to the flux ratio; they are notably able to mimic the small astrometric motions caused by sub-stellar companions. As such, during our RV observations with HARPS-N special care was taken to produce and analyse the cross correlation function (CCF) profiles of the high-S/N spectra (ranging from 40 to 70), which were reduced using the HARPS-N data-reduction software (DRS; Lovis & Pepe 2007), to identify the double-peaked profiles of SB2 configurations and exclude such stars from subsequent observations.

Amongst the 14 stars with Gaia DR3 astrometric candidate solutions included in our sample, we identify six stars as SB2 systems generating astrometric false-positive solutions; for these, we show the HARPS-N CCF with a clear double-peak profile in Fig. 1 . In Table A.1 we also report the candidate Gaia non-single-star orbital period of $P_{\rm NSS}$. We note that two of these stars, PM J08079+2651 and TYC 1546-519-1, have a Gaia DR3 SB1 solution.

Having found six astrophysical false positives amongst the 14 Gaia DR3 candidate solutions, we can derive a 43^{+13}_{-11}% binary contamination fraction assuming binomial uncertainties, a value that is notably higher than the ~10% estimated in Holl et al. (2023) but instead fully compatible within 1σ with the more recent ~32% derived by Stefánsson et al. (2025).

4. Gaia candidates validation and confirmation

Having identified and excluded six new false positives among the 14 Gaia astrometric candidate orbits in our sample, in this section we focus on the eight remaining sub-stellar Gaia astrometric candidates validated by a single-peaked CCF profile. As mentioned in Sect. 3, the spectra collected were reduced using the HARPS-N DRS (Lovis & Pepe 2007), while the RV extraction was performed using the Template-Enhanced Radial velocity Re-analysis Application pipeline (TERRA, Anglada-Escudé & Butler 2012). All RV measurements collected, as well as all activity indicators analysed in the following, are listed in Table 1, while we list the number of the measurements collected, the observational time span, coverage of the NSS orbital period, average RV uncertainty, and weighted root mean square (w.r.m.s) in Table A.3.

To search for the massive long-period companions in the HARPS-N RV time series we collected during our observations, we calculated the generalised Lomb–Scargle periodogram (GLS, Zechmeister & Kürster 2009) of the RVs to identify significant signals that have a bootstrap false-alarm probability (FAP) lower than 0.1%. At the same time, we analyse the activity indices' time series derived as discussed in Sect. 2 to investigate the origin of any stellar activity for the observed significant RV signals. Similarly, we inspected the available All Sky Automated Survey (ASAS, Pojmanski 2002), Transiting Exoplanet Survey Satellite (TESS, Ricker et al. 2015), and Gaia light curves for each star in the sample to identify, via GLS and autocorrelation functions

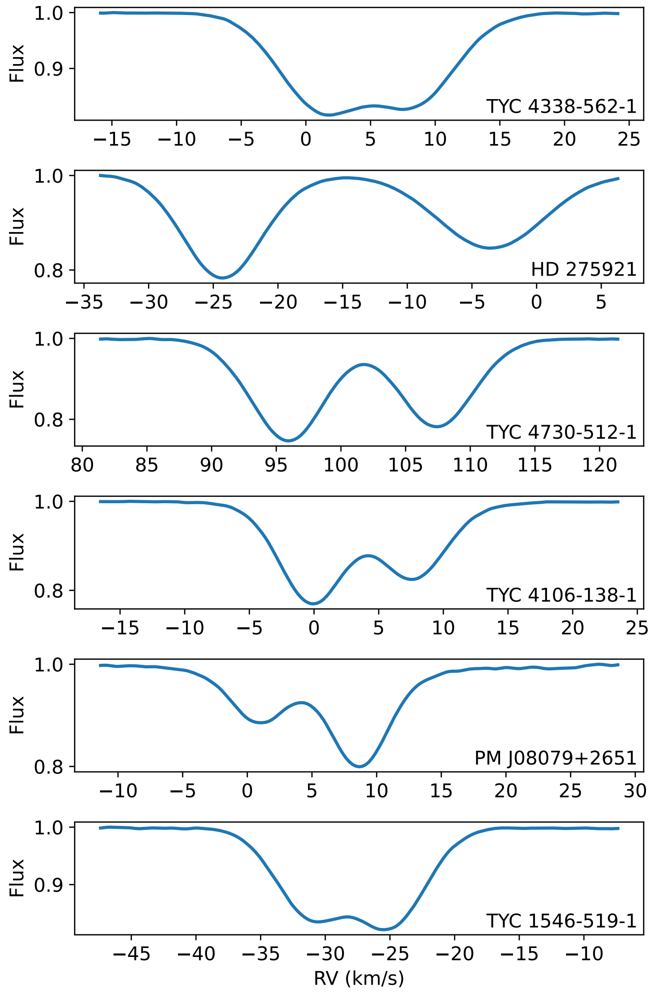

Fig. 1. HARPS-N cross correlation function profiles of the six stars in the sample identified as binaries mimicking sub-stellar astrometric motion.

[2] https://actin2.readthedocs.io/en/latest/index.html

Table 1. HARPS-N measurements for the stars discussed in this work.

Star	BJD	T_{exp} (s)	RV ($km\,s^{-1}$)	CCF FWHM ($km\,s^{-1}$)	CCF BIS ($km\,s^{-1}$)	S_{MW}	Hα	Na I
2MASS J20570943+1406590	2460224.50	1800	6.7426 ± 0.0059	5.9003	0.0358	0.1662 ± 0.0153	0.1547 ± 0.0023	0.3018 ± 0.0044
2MASS J20570943+1406590	2460227.54	1800	6.7014 ± 0.0030	5.8662	0.0089	0.2156 ± 0.0083	0.1541 ± 0.0015	0.2982 ± 0.0029
2MASS J20570943+1406590	2460236.46	1800	6.5794 ± 0.0023	5.8740	0.0132	0.1469 ± 0.0066	0.1552 ± 0.0014	0.2954 ± 0.0027
2MASS J20570943+1406590	2460244.45	1800	6.4603 ± 0.0024	5.8894	0.0322	0.1520 ± 0.0057	0.1575 ± 0.0015	0.2968 ± 0.0027
2MASS J20570943+1406590	2460245.45	1800	6.4460 ± 0.0027	5.8817	0.0129	0.1476 ± 0.0061	0.1565 ± 0.0016	0.3041 ± 0.0029
...	...	...	...	...	...	...	...	...

Notes. Data are available at the CDS. A selection is shown here for guidance regarding form and content.

(McQuillan et al. 2013), any modulation due to stellar activity compatible with the timeline of the photometric observations. When appropriate, we also modelled the available light curves with Gaussian-process (GP) and quasi-periodic kernel fits to derive the stellar rotational period, P_{rot}, in order to inform future searches for close-in companions. Unless otherwise stated, our HARPS-N observations represent the first RV time series available for these stars, as no other public RV measurements are found in the literature or in the archives.

For each star for which we identify significant and robust RV signals, we searched for the best-fit orbital solution using the Python tool `PyORBIT`[3] (Malavolta et al. 2016, 2018), a package for the Markov chain Monte Carlo (MCMC) modelling of RV and activity indices' time series based on the optimisation algorithm `PyDE` (Storn & Price 1997) and the MCMC sampler `emcee` (Foreman-Mackey et al. 2013). The free parameters we fitted for are orbital period, P; semi-amplitude, K; mean longitude, λ_0; $\sqrt{e_b}\sin\omega_b$; $\sqrt{e_b}\cos\omega_b$; and finally a zero-point RV term, γ, and uncorrelated stellar jitter term, j, for each RV dataset. We set a uniform prior on P based on the astrometric candidate period nominal value P_{NSS}, bounding the fitted P between 0.8 and 1.2 times this value. We detail the results of our analysis for each star in the following subsections, presented in decreasing order of HARPS-N coverage of the astrometric candidate orbital period, showing the orbital solutions in Fig. 2, and listing the best-fit parameters in Table A.3. In the same table we additionally report the relevant NSS candidate-solution orbital parameters, as well as the companion-mass lower value of M_{NSS} corresponding to the lower confidence level (assuming no flux contamination) and true mass estimates ($M_{b,i_{NSS}}$) from our RV minimum mass values by adopting the NSS orbital inclination value to provide an additional comparison between our RV-only solution and the NSS candidate parameters. Unless otherwise stated in the following subsections, we generally find our RV-only best-fit parameters to be within 2σ of the NSS candidate-solution values.

4.1. 2MASS J20570943+1406590

The 2MASS J20570943+1406590 K4 star is located 110 pc from the Sun. No long-period modulation is evident from the available ASAS and TESS (Sectors 55 and 82) light curves. The Gaia DR3 NSS solution is compatible with the presence of a companion that has an orbital period of 280.76 ± 3.16 d, eccentricity of 0.33 ± 0.13, and, assuming a 0.72 $M_\odot$ mass for the host star, a lower 1-σ confidence level on true mass (hereinafter referred to as lower M_{NSS} for simplicity) of ~38.78 M_{Jup} (Gaia Collaboration 2022).

In the top row of Fig. B.1 we show the HARPS-N RV time series and GLS periodogram, from which we find a highly significant principal peak at ~285 d with FAP=$4\cdot10^{-17}$%. We find no correlation among this RV signal, the CCF full width at half maximum (FWHM), and the CCF bisector inverse span (BIS; shown in the third and fourth rows of Fig. B.1) and any of the activity indices we derived with `ACTIN2` (see Sect. 2; and shown in the fifth to eighth rows of Fig. B.1). In fact, the strongest correlation we find is the one between the RV time series and Na I, which has a Pearson correlation coefficient of ρ=0.43, a p-value of 0.01 indicating only moderate correlation, and an activity-index GLS periodogram with a FAP=0.05% principal peak located at ~356 d. We therefore excluded a stellar activity origin for the large-amplitude RV signal.

When searching for the best-fit orbital solution using `PyORBIT`, we found a single-Keplerian orbit with period of 281.89 ± 0.09 d, semi-amplitude of $1233.31^{+3.99}_{-3.91}$ m s^{-1}, and eccentricity of 0.313 ± 0.002. Using the host star's mass value of $0.689^{+0.031}_{-0.030}$ $M_\odot$ we obtained from the SED fit detailed in Sect. 2, we derived a companion minimum mass of $30.32^{+0.84}_{-0.91}$ M_{Jup} and an orbital semi-major axis of 0.75 ± 0.01 au. The post-Keplerian-fit residual RVs' GLS periodogram, shown in the second row of Fig. B.1, exhibits no significant signal (with the residual principal peak at ~24 d having a 10% FAP) nor any strong correlation with the analysed activity indices.

Notably, our RV best-fit solution is highly compatible with the Gaia DR3 astrometric candidate. We therefore validated the Gaia DR3 solution and assessed the observed astrometric motion of the star as caused by the presence of the low-mass BD companion described in this section.

4.2. HIP 105707

The HIP 105707 K7 star has a distance of 50 pc from the Sun. Our analysis of the ASAS and TESS (Sectors 15, 55, and 56) light curves reveals no significant long-term activity. However, a modulation is detected in the TESS data on a timescale of either ~4.4 days (from a single-term Lomb–Scargle and GP fit) or ~8.8 days (from a multi-term Lomb–Scargle fit), suggesting activity on shorter timescales. The NSS solution for this star finds a candidate companion on a 687.71 ± 12.67 d orbit with an eccentricity of 0.51 ± 0.03 and lower M_{NSS} ~23.77 M_{Jup} assuming a primary mass of 0.70 $M_\odot$.

Our HARPS-N observations (see Fig. B.2) exhibit clear long-term eccentric Keplerian-like behaviour, with a principal periodogram peak of ~604 d and a low FAp-value of $1.18\cdot10^{-23}$%. Most of the activity indices show low-to-moderate correlation with the RVs, with the only exception being the high correlation present (ρ = −0.88, p-value= 0) with the Hα index. However, the observed RV variation (~1335 m s^{-1}) is incompatible with an activity-only origin and is corroborated by the astrometric candidate solution, which is mostly insensitive to such activity signals (see e.g. Lagrange et al. 2011 and Meunier et al. 2020); having an orbital period of the same order of magnitude as the observed

[3] `https://github.com/LucaMalavolta/PyORBIT`

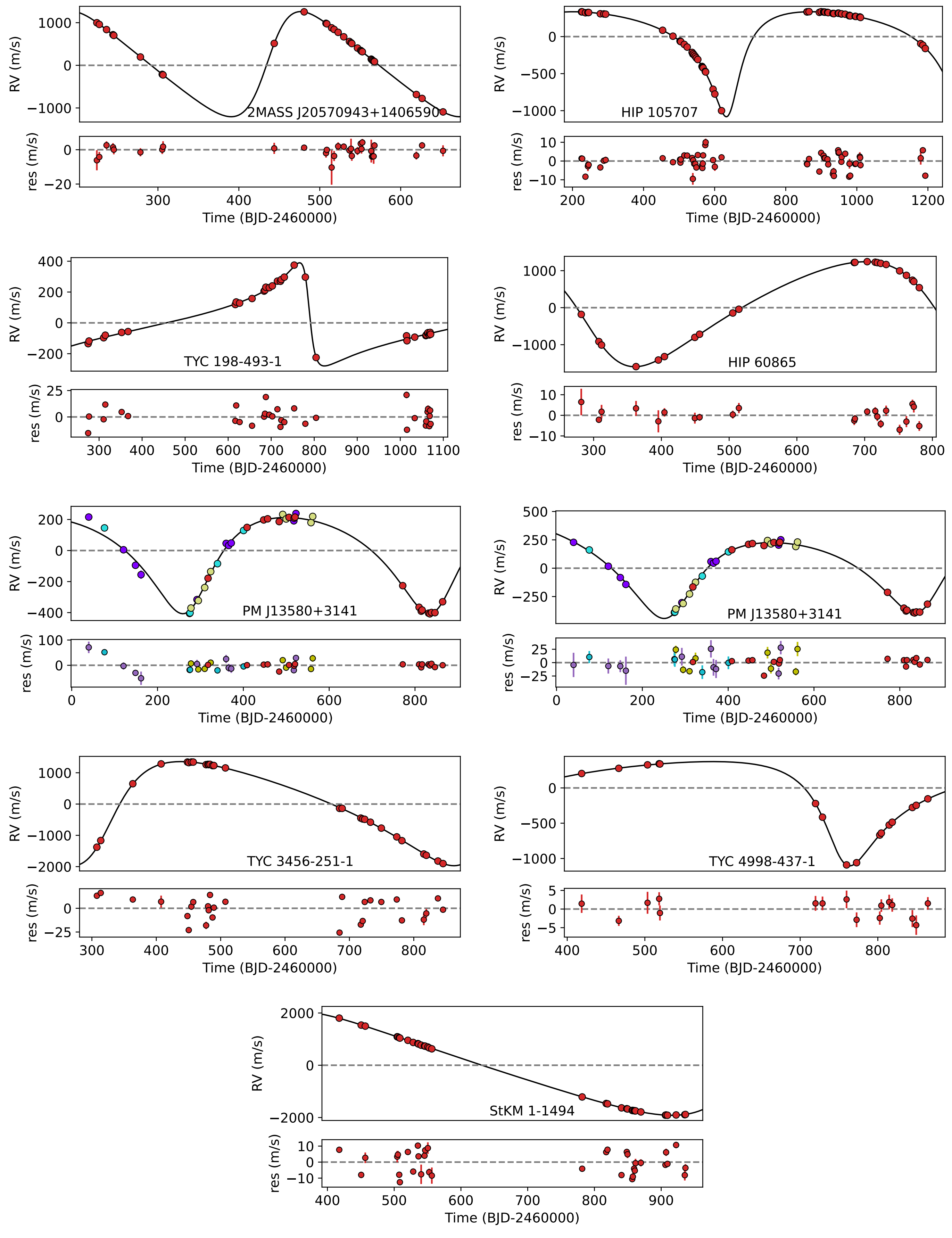

Fig. 2. Radial velocity orbital fits for the stars discussed in this work. For all stars, the top panel shows the best-fit solution over the HARPS-N (red circles) data, while the bottom panel shows the post-Keplerian fit residuals. In the two figures shown for PM J13580+3141 (single-Keplerian and Keplerian with quadratic trend solutions, respectively), literature HPF, FIES, and NEID data are shown as purple, cyan, and yellow circles.

RV signal and a companion-induced origin for the RV variation is preferred.

Our Keplerian solution is highly compatible with the astrometric candidate solution; it has an orbital period of $668.76^{+2.54}_{-2.60}$ d, semi-amplitude of $707.60^{+7.78}_{-7.15}$ m s^{-1}, and eccentricity 0.563 ± 0.005. From the $0.707^{+0.028}_{-0.026}$ $M_\odot$ host- star mass we derived from our SED fit, we infer a companion minimum mass of 20.34 ± 0.58 $M_{\rm Jup}$ and a semi-major axis of 1.34 ± 0.02 au.

We additionally note that HIP 105707 is one of the two stars among those discussed in this work for which the PMa value is present in the HGCA. As such, we performed a combined fit of the HARPS-N RV observations and PMa measurements using the Python code `orvara` (Brandt et al. 2021). For the detected companion we find a semi-major axis of 1.35 ± 0.02 au, an eccentricity of $0.563^{+0.006}_{-0.005}$, and an orbital inclination of 100^{+16}_{-17} deg, which we note to be in agreement with the NSS value within 1.5σ and a dynamical mass of $21.13^{+1.80}_{-0.94}$ $M_{\rm Jup}$. This joint RV-PMa solution is in notable agreement with the RV-only one, with the added benefit of providing a true mass value confirming the BD nature of the detected companion.

4.3. TYC 198-493-1

The TYC 198-493-1 K0 is a star located 78 pc from the Sun. Although neither the ASAS nor TESS (Sectors 07, 34 and 61) data exhibit long-term modulation, they show clear short-term modulation suggesting moderate activity, and we derive a rotational period of 12 ± 4days and 12.9 ± 0.4 d, respectively. The NSS solution for this star suggests the presence of a companion with an orbital period of 722.60 ± 8.79 d and high 0.75 ± 0.07 eccentricity and, assuming a host-star mass of 0.83 $M_\odot$, a lower $M_{\rm NSS}$ ~49 $M_{\rm Jup}$.

As for HIP 60865, four archival SOPHIE RV measurements are available, but their ~0.1 km s^{-1} uncertainty renders them unsuitable for our analysis. As shown in Fig. B.3, a large long-term Keplerian variation is present in the data. Apart from a strong 1 d peak in the periodogram, the principal peak is located at ~658 d and has a FAP of 0.18%. No strong correlation between RVs and activity indices is evident, with the exception of a moderate correlation ($|\rho|$ ~0.58 with a p-value of < 0.001) being present between RVs and Na I. We find the data to be best described by a Keplerian model having an orbital period of $718.67^{+6.41}_{-6.35}$ d, semi-amplitude $335.09^{+4.21}_{-3.89}$, and high eccentricity of 0.739 ± 0.006. This solution, given the $0.817^{+0.037}_{-0.035}$ $M_\odot$ host-star mass obtained from our SED fit, corresponds to a 8.63 ± 2.52 $M_{\rm Jup}$ minimum mass and $1.47^{+0.19}_{-0.23}$ au semi-major axis for the companion.

We note that our value of $M \sin i$ is much lower than the minimum NSS true mass estimate of 49 $M_{\rm Jup}$. However, assuming the NSS orbital inclination value of 14.62 ± 18.02 deg our $M \sin i$ would correspond to a true dynamical mass of 34.19 ± 21.72, which is in full agreement with the NSS true mass estimate.

4.4. HIP 60865

The HIP 60865 K7 star is at a distance of 72 pc. No long-period modulation is evident from the available ASAS and TESS (Sectors 22 and 49) light curves. The Gaia DR3 NSS solution for this star suggests the existence of a companion with an orbital period of 500.69 ± 4.88 d, an eccentricity of 0.25 ± 0.06, and, by assuming a host-star mass of 0.67 $M_\odot$, a lower $M_{\rm NSS} of$ ~46.97 $M_{\rm Jup}$. Although five archival SOPHIE measurements are available, their ~0.1 km s^{-1} uncertainty makes them unsuitable for RV orbital fitting in the presence of our high-precision HARPS-N measurements and they are therefore not included in our analysis.

The GLS periodogram computed for our HARPS-N data points, shown in the top row of Fig. B.4, exhibits a principal peak of ~620 d with a highly significant FAP of $1.1 \cdot 10^{-14}$%. While the majority of the activity indices (third to eighth row of Fig. B.4) show neither significant peaks nor correlations with the RVs, an exception is represented by the Hα index, which has $\rho = -0.91$ and a zero p-value, and for which we find a significant (FAP=$1.6 \cdot 10^{-4}$%) peak at the same period of the aforementioned RV signal. Although this coinciding periodicity could, in principle, indicate an activity origin for the proposed signal, we must note that the very large variation observed in the RV time series (~2835 m s^{-1} peak-to-valley) is incompatible with any expected activity-induced Doppler signal for such an old star. Moreover, the compatibility between the RV periodogram principal peak and the ~500 d orbital period proposed by the Gaia DR3 NSS solution, which is by nature mostly insensitive to signals induced by stellar activity, suggests a companion origin for the observed RV variation. As such, HIP 60865 may have an activity cycle coinciding with the orbital period of its massive companion, a situation similar to that of the Solar System, in which the orbital period of Jupiter coincides with the ~11 yr solar sunspot cycle (which itself produces an RV variation of 4.98 ± 1.44 m s^{-1}, as detailed in Lanza et al. 2016).

We find the data to be best described by a Keplerian solution having an orbital period of 528.08 ± 0.39 d, semi-amplitude of $1418.62^{+1.81}_{-1.76}$ m s^{-1}, and eccentricity of 0.261 ± 0.002. By using the 0.683 ± 0.026 $M_\odot$ value for host-star mass obtained by our SED fit (see Sect. 2), we were able to derive a minimum mass of 43.93 ± 1.09 $M_{\rm Jup}$ and a semi-major axis value of 1.15 ± 0.01 au for the companion. We find no significant signal in the residual RVs (second row of Fig. B.4), with the principal peak at ~1 d having a 0.3% FAP, as well as no correlation with the activity indices considered. Once again, our RV solution is found to be in strong agreement with the astrometric candidate proposed in Gaia DR3, with the notable exception of a larger RV-only orbital period within 5.6σ of the NSS candidate value.

This star is also included in the HGCA, and we therefore perform a combined RV ad PMa fit with `orvara,` as done for 4.2, finding for the detected companion a semi-major axis of 1.15 ± 0.2 au, eccentricity of 0.260 ± 0.002, true dynamical mass of $46.1^{+3.8}_{-2.2}$ $M_{\rm Jup}$, and orbital inclination of 76^{+18}_{-13} deg agreeing with $i_{\rm NSS}$ within 0.4σ.

4.5. PM J13580+3141

The K7 star PM J13580+3141 has an estimated distance of 73 pc from the Sun. No long-term stellar modulation is evident from the ASAS and TESS (Sectors 23 and 50) data, but we can infer a rotation period of 13.2 ± 0.3 d from ASAS; from TESS we obtain $7.0^{+0.7}_{-0.5}$ d, which is nearly half of the ASAS value, and a similar short-period variability (6.6 d) is present in the Gaia photometry. The NSS solution is compatible with a companion with lower a $M_{\rm NSS} of$ ~11.66 $M_{\rm Jup}$ (assuming a host-star mass of 0.64 $M_\odot$) on a 564.02 ± 11.19 d orbit with an eccentricity of 0.51 ± 0.19.

This candidate companion was first validated as Gaia-4 b by Stefánsson et al. (2025) by jointly fitting the Gaia astrometric orbit and a total of 23 RV data points collected with the HPF (Mahadevan et al. 2014), NEID (Schwab et al. 2016), and FIES (Telting et al. 2014) spectrographs. These RV measurements allowed for the validation of the astrometric candidate, which was found to be a giant planet with a true mass of $11.80^{+0.73}_{-0.66}$ $M_{\rm Jup}$ on a $571.3^{+1.4}_{-1.3}$ d orbit with an eccentricity of $0.338^{+0.026}_{-0.023}$, in perfect agreement with the astrometric candidate orbit.

Our HARPS-N time series exhibit a clear Keplerian-like variation, with a periodogram (see Fig. B.5) featuring a highly significant (FAP=$1.3{\cdot}10^{-9}$%) long-periodicity region starting at ∼500 d; this is clearly compatible with the long-period planet Gaia-4 b. Our HARPS-N time series covers a significant portion of the orbit of Gaia-4 b (∼96%) and is characterised by a significantly lower median uncertainty than the ∼12 m s^{-1} median error of the RV time series analysed in Stefánsson et al. (2025), allowing for an updated characterisation of the planetary companion orbit.

When combining our HARPS-N time series with the literature measurements, we find, for Gaia-4 b, an updated Keplerian solution (shown in the fifth panel of Fig. 2) with an orbital period of $574.46^{+3.06}_{-2.83}$ d, semi-amplitude of $309.97^{+2.70}_{-2.47}$ m s^{-1}, and eccentricity of $0.336^{+0.013}_{-0.014}$. While no significant residual periodogram peak is present, the post-fit residual time series feature some disagreement between the RV model and the first few HPF and FIES data points, resulting in significant residual scatter in the first descending portion of the RV model. Such scatter could, in principle, be produced by an outer massive companion imposing a long-term trend in the RV data. As such, we performed an additional orbital fit in which we added a quadratic trend to the Keplerian model, resulting in a solution that is marginally statistically preferred (see sixth panel of Fig. 2), with a difference in the Bayesian information criterion of 9.11. As such, we adopted this solution, in which we find an orbital period of $588.58^{+2.15}_{-2.50}$ d, semi-amplitude of $347.42^{+2.15}_{-2.75}$ m s^{-1}, and eccentricity of $0.318^{+0.011}_{-0.012}$, with quadratic trend coefficients of -0.21 ± 0.06 m s^{-1} d^{-1} and 0.0006 ± 0.0001 m s^{-1} d^{-2}. From the host mass of $0.652^{+0.027}_{-0.025}$ $M_\odot$ obtained from the SED fit, we derive a minimum planetary mass of 10.30 ± 0.45 $M_{\rm Jup}$ and semi-major axis of 1.20 ± 0.02 au. The post-fit residuals have a w.r.m.s. of ∼7 m s^{-1} and no significant periodogram peak.

While we note that the orbital period obtained from our RV-only solution is slightly less constrained than the joint RV and Gaia solution presented in Stefánsson et al. (2025), it is instead better constrained than the RV-only value of the cited work (513^{+21}_{-16} d), as a result of both the extended observational time span and the higher precision HARPS-N measurement (with an average uncertainty of 2.95 m s^{-1} compared to the 16, 8.3, and 12.4 m s^{-1} of the HPF, NEID, and FIES time series, respectively). The robust characterisation of the quadratic trend and its source requires additional observation and will therefore be the subject of a future analysis.

4.6. TYC 3456-251-1

The TYC 3456-251-1 G9 star is located at a distance of 151 pc. The available ASAS and TESS (Sectors 22 and 49) light curves do not exhibit long-term modulation. For this star, the Gaia DR3 NSS catalogue is compatible with the presence of a massive companion with an orbital period of 593.26 ± 7.89 d and eccentricity 0.14 ± 0.07, which, by assuming a host mass of 0.87 $M_\odot$, implies lower $M_{\rm NSS}$ ∼52.3 $M_{\rm Jup}$.

As shown in Fig. B.6, the GLS periodogram for our HARPS-N RV time series is characterised by a long-period (>400 d) signal with a FAP of $1.4{\cdot}10^{-11}$%, which is consistent with the proposed astrometric candidate. The only activity index exhibiting strong correlation with the RV time series is Na I ($\rho = -0.68$ and zero p-value), for which we find a peak periodicity of ∼488 d with a FAP of $1{\cdot}10^{-6}$%. As discussed in Sections 4.2 and 4.4 for stars HIP 105707 and HIP 60865, we refute an activity-only origin for the aforementioned long-period signal by virtue of the large variation of the RV time series (∼3200 m s^{-1}) and the fact that the periodicity of the RV signal is consistent with the proposed astrometric orbital solution.

When performing an orbital fit of the data, we found a best-fit Keplerian solution with an orbital period of $592.66^{+4.92}_{-4.31}$ d, semi-amplitude of $1662.35^{+17.60}_{-15.22}$ m s^{-1}, and moderate eccentricity of 0.387 ± 0.003. This best-fit solution, using the host-star mass of $0.854^{+0.050}_{-0.041}$ $M_\odot$ obtained by our SED fit, would correspond to a minimum companion mass of $59.52^{+2.46}_{-2.38}$ $M_{\rm Jup}$ and a semi-major axis of 1.34 ± 0.03 au. We find our solution to be in strong agreement with the Gaia DR3 NSS candidate solution, with the notable exceptions of significantly higher eccentricity and argument of periastron values from our solution; these are, respectively, within 3.5σ and 6.2σ of the NSS solution. While the post-fit residual time series exhibit a relatively high scatter and a w.r.m.s. of 11 m s^{-1}, no significant peak is present in the current data, with the principal residual peak being located at ∼8.6 d and having a FAP of 0.8%.

4.7. TYC 4998-437-1

The K1 star TYC 4998-437-1 is located at 132 pc from the Sun. No long-period modulation is clear from the ASAS and TESS (Sectors 51 and 91) light curves. For this star, the Gaia DR3 NSS solution suggests a candidate companion on a 526.14 ± 23.10 d orbit with an eccentricity of 0.43 ± 0.16, from which lower $M_{\rm NSS}$ ∼33.61 $M_{\rm Jup}$ can be estimated assuming a mass of 0.81 $M_\odot$ for the host star (Gaia Collaboration 2022).

Although the HARPS-N RV time series (top row of Fig. B.7) shows a very clear variation hinting at a Keplerian-like long-period behaviour, the corresponding GLS periodogram lacks any highly significant peak, with its 495 d principal peak having a FAP of 0.20%. It is nevertheless compatible with the astrometric candidate orbit. We find moderate correlation between RVs and most of the activity indices, with the significant exception of the strong correlation found with Hα ($\rho = 0.83$ with a zero p-value). However, we once again stress that the amplitude of the observed RV variation (∼1433 m s^{-1} peak-to-valley) is too large to be induced by activity alone, with the astrometric candidate additionally motivating the search for a companion causing the RV variation.

The orbital fit we performed on the data results in a best-fit Keplerian with a $558.67^{+2.80}_{-2.47}$ d period, $738.92^{+1.75}_{-1.87}$ m s^{-1} semi-amplitude, and 0.557 ± 0.002 eccentricity. From this, using our SED-derived host-star mass of $0.856^{+0.043}_{-0.035}$ $M_\odot$, we find a companion minimum mass value of $22.80^{+0.75}_{-0.77}$ $M_{\rm Jup}$ and semi-major axis of 1.27 ± 0.02 au. Once again, we note the high agreement between our RV solution and the astrometric candidate orbit, and no significant peak is present in the residual time series.

4.8. StKM 1-1494

The StKM 1-1494 M0 star has a distance of 27 pc. No TESS data are available; however, we infer a possible rotational period of 6 ± 3 d from the ASAS light curve and a ∼12 d periodicity from Gaia photometry, which may be aliases of each other. The Gaia DR3 solution has an orbital period of 829.40 ± 1.76 d and an eccentricity of 0.328 ± 0.006, corresponding to a lower $M_{\rm NSS} of$ ∼64.2 $M_{\rm Jup}$ and assuming a host mass of 0.58 $M_\odot$.

This candidate companion was recently confirmed through direct-imaging observations performed with the GRAVITY

(GRAVITY Collaboration et al. 2017) near-infrared interferometer as detailed in Winterhalder et al. (2024). GRAVITY allowed for the direct imaging of the candidate companion, which, combined with the Gaia orbital solution, allowed its validation and characterisation with an orbital period of 828.2 ± 1.6 d, eccentricity of 0.331 ± 0.006, and mass of $67.5 \pm 1.2\ M_{\rm Jup}$. We additionally note that this star has an SB1 solution in DR3, although the short period of 7.9 days and large amplitudes in excess of 1.8 km/s suggest incorrect identification of the correct period value due to, for example, aliasing effects.

Our HARPS-N observations cover ~62% of the candidate orbital period, therefore only allowing the detection of a large trend in the data with recent hints of curvature. We find a total RV variation of 3584 m s^{-1} and a significant GLS periodogram long-period (>800 d) signal with a $3{\cdot}10^{-27}$% FAP. Although a robust solution would clearly require a larger orbital coverage, the most recent data manage to sample the minimum of the RV oscillation, allowing us to perform an RV fit to provide a first assessment of the spectroscopic orbit of the detected brown dwarf. We find a best-fit solution with an orbital period of $789.26^{+10.08}_{-11.25}$ d, semi-amplitude of $1984.95^{+11.16}_{-18.19}$ m s^{-1}, and eccentricity of 0.335 ± 0.007. We note that our solution is characterised by a significantly shorter period than the NSS candidate one (within 4.15σ). This disagreement is likely a result of the incomplete coverage of the orbital period provided by our HARPS-N data, again highlighting how further observations can improve the orbital characterisation of this companion. From the host-star mass of $0.584 \pm 0.027\ M_\odot$ we infer a minimum companion mass of $63.35^{+1.93}_{-2.03}\ M_{\rm Jup}$ and semi-major axis of 1.44 ± 0.02 au. The residual time series features a principal peak of ~15 d with a 0.01% FAP coinciding with significant peaks in the FWHM, Ca II, Hα, suggesting an activity origin for the residual RV scatter.

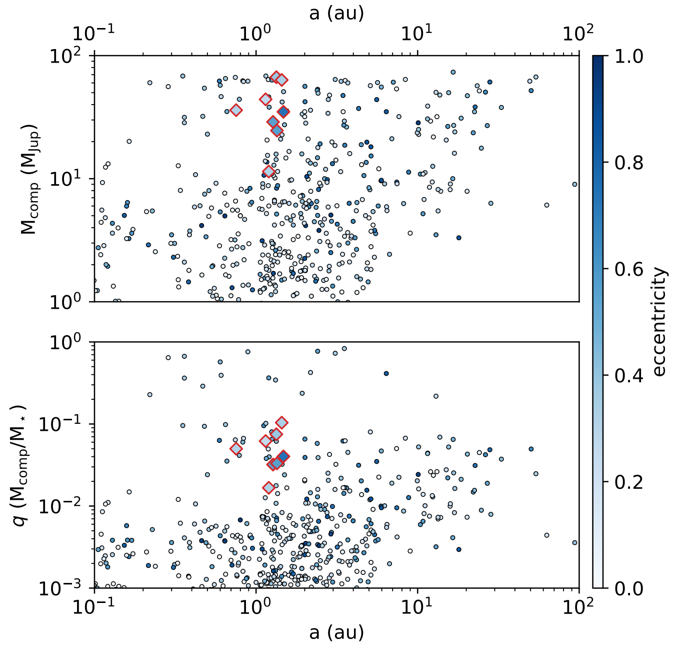

Fig. 3. Location of the eight companions discussed in this work (red-bordered diamonds) in the known exoplanet and brown dwarf (black-bordered circles) single-companion population, colour-coded according to orbital eccentricity. *Top panel*: Companion mass versus orbital separation. *Bottom panel*: Companion-to-host mass ratio, q, versus orbital separation.

5. Discussions and conclusions

In this paper we present the first results of an ongoing RV survey conducted with HARPS-N on 35 stars hosting cold Jupiters or low-mass BDs. Specifically, we focused on the 14 stars in the sample characterised by Gaia DR3 non-single-star solutions compatible with the presence of such massive companions in order to identify astrophysical false positives in the NSS solutions and provide RV confirmation and characterisation of the remaining validated candidates.

We identified six NSS solutions in the sample as astrophysical false positives originating from an unresolved SB2 mimicking sub-stellar astrometric motion, from which we can estimate a 43^{+13}_{-11}% binary contamination fraction in our sample. Notably, this value is higher than preliminary contamination estimations reported in the literature, such as the ~10% derived in Holl et al. (2023), but it is instead in agreement with a more recent and higher value of ~32% (see e.g. Stefánsson et al. 2025). This result highlights the critical role of RV follow-up observations in validating astrometric candidates. We additionally note that these false positives tend to be the furthest away stars in our sample. Indeed, five out of the six targets with parallaxes lower than 7.5 mas in the sample are found to be binaries. Moreover, five out of six false positives were found around stars with masses above $0.9\ M_\odot$, in line with the frequency of binaries growing with the primary mass (see e.g. Moe & Di Stefano 2017).

The HARPS-N data collected in our survey allowed us to validate and confirm the eight remaining astrometric sub-stellar candidates in our sample, finding RV best-fit solutions compatible with giant and BD companions with minimum masses ranging from 8 $M_{\rm Jup}$ to 62 $M_{\rm Jup}$ and semi-major axes from 0.75 au to 1.42 au. While we additionally note that two companions have recently been confirmed by other observational efforts, namely RV for PM J13580+3141 (Stefánsson et al. 2025) and imaging data for StKM 1-149 (Winterhalder et al. 2024), our high-precision HARPS-N measurements allow for updated orbital solutions. In general, our solutions are in good agreement with the NSS astrometric solutions, and by adopting the NSS orbital inclination to derive true mass estimates from our $M \sin i$ we obtain values higher than or compatible with the NSS minimum companion mass.

Finally, in Fig. 3 we show the location of the eight companions analysed in this work, represented with their true mass estimates $M_{b,i_{\rm NSS}}$, in the known single-companion brown dwarf and exoplanetary population with available true mass estimates, from which we can note that the more massive of these companions are found to be populating the BD desert (<5 au, see Marcy & Butler 2000 and Sahlmann et al. 2011).

As an additional testament to the continued impact of Gaia astrometric measurements on other techniques, we note how some of the astrometric candidate solutions discussed in this work have orbital periods compatible with activity cycles as detected by the spectroscopical analysis performed on our HARPS-N data, specifically for stars HIP 60865, HIP 105707, TYC 3456-251-1, and TYC 4998-437-1. As the astrometric method is by nature mostly insensitive to signals induced by stellar activity, the astrometric identification of a candidate's orbital period can be a key asset in refuting a stellar activity origin for observed RV signals. Although the Keplerian nature of the observed RV signals presented in this work is clear from their very large RV amplitudes alone, we can foresee a significant role in the near future for Gaia astrometric solutions in solving more dubious cases such as those with smaller RV amplitudes, which by itself could easily remain ambiguous, as further RV follow-up of Gaia candidates is conducted.

While the present work has focused solely on the validation and confirmation of astrometric candidates in our 35-star HARPS-N sample, a final key objective of our survey, namely the search for low-mass inner companions in the presence of outer massive companions with astrometric-derived true masses, is ongoing and will be the subject of forthcoming papers. As the search for inner companions continues within our stellar sample, we will be able to provide an updated assessment of ordered system demographics based on outer companion true masses as provided by astrometry, highlighting once more the growing role of multi-technique observations in the exoplanetary landscape.

6. Data availability

Full Table 1 is available in electronic form at the CDS via anonymous ftp to `cdsarc.u-strasbg.fr` (`130.79.128.5`) or via `http://cdsweb.u-strasbg.fr/cgi-bin/qcat?J/A+A/`.

Acknowledgements. The authors wish to thank the referee, Dr. C. Babusiaux, for the useful comments which significantly improved the manuscript quality. This work is based on observations made with the Italian *Telescopio Nazionale Galileo* (TNG), operated on the island of La Palma by the INAF - *Fundación Galileo Galilei* at the *Roque de Los Muchachos* Observatory of the *Instituto de Astrofísica de Canarias* (IAC). We acknowledge the Italian center for Astronomical Archives (IA2, `https://www.ia2.inaf.it`), part of the Italian National Institute for Astrophysics (INAF), for providing technical assistance, services and supporting activities of the GAPS collaboration. This work has made use of data from the European Space Agency (ESA) mission *Gaia* (`https://www.cosmos.esa.int/gaia`), processed by the *Gaia* Data Processing and Analysis Consortium (DPAC, `https://www.cosmos.esa.int/web/gaia/dpac/consortium`). Funding for the DPAC has been provided by national institutions, in particular, the institutions participating in the *Gaia* Multilateral Agreement. This research has made extensive use of the NASA-ADS, SIMBAD and Vizier databases, operated at CDS, Strasbourg, France. M.P. acknowledges support from the European Union – NextGenerationEU (PRIN MUR 2022 20229R43BH), the "Programma di Ricerca Fondamentale INAF 2023", and from ASI-INAF agreement no. 2025-10-HH.0 "Partecipazione Italiana al Gaia DPAC - Supporto alle attività di responsabilità del team scientifico". J.M. acknowledges support from the Italian Ministero dell'Università e della Ricerca and the European Union – Next Generation EU through project PRIN 2022 PM4JLH "Know your little neighbours: characterising low-mass stars and planets in the Solar neighbourhood". L.N. acknowledges financial contribution from the INAF Large Grant 2023 "EXODEMO". L.M. acknowledges the financial contribution from the PRIN MUR 2022 project 2022J4H55R.

References

Adamow, M. M. 2017, in American Astronomical Society Meeting Abstracts, Vol. 230, American Astronomical Society Meeting Abstracts #230, 216.07
Almeida-Fernandes, F. & Rocha-Pinto, H. J. 2018, MNRAS, 476, 184
Anders, F., Khalatyan, A., Queiroz, A. B. A., et al. 2022, A&A, 658, A91
Anglada-Escudé, G. & Butler, R. P. 2012, ApJS, 200, 15
Armitage, P. J. & Bonnell, I. A. 2002, MNRAS, 330, L11
Barbato, D., Sozzetti, A., Desidera, S., et al. 2018, A&A, 615, A175
Biazzo, K., D'Orazi, V., Desidera, S., et al. 2022, A&A, 664, A161
Bitsch, B. & Izidoro, A. 2023, A&A, 674, A178
Bonomo, A. S., Dumusque, X., Massa, A., et al. 2023, A&A, 677, A33
Bonomo, A. S., Naponiello, L., Pezzetta, E., et al. 2025, A&A, 700, A126
Brandt, T. D. 2021, ApJS, 254, 42
Brandt, T. D., Dupuy, T. J., Li, Y., et al. 2021, AJ, 162, 186
Bryan, M. L., Knutson, H. A., Lee, E. J., et al. 2019, AJ, 157, 52
Bryan, M. L. & Lee, E. J. 2024, ApJ, 968, L25
Casertano, S., Lattanzi, M. G., Sozzetti, A., et al. 2008, A&A, 482, 699
Chabrier, G., Johansen, A., Janson, M., & Rafikov, R. 2014, in Protostars and Planets VI, ed. H. Beuther, R. S. Klessen, C. P. Dullemond, & T. Henning, 619–642
Chambers, K. C., Magnier, E. A., Metcalfe, N., et al. 2016, arXiv e-prints, arXiv:1612.05560
Choi, J., Dotter, A., Conroy, C., et al. 2016, ApJ, 823, 102
Cosentino, R., Lovis, C., Pepe, F., et al. 2012, in Society of Photo-Optical Instrumentation Engineers (SPIE) Conference Series, Vol. 8446, Ground-based and Airborne Instrumentation for Astronomy IV, ed. I. S. McLean, S. K. Ramsay, & H. Takami, 84461V
Covino, E., Esposito, M., Barbieri, M., et al. 2013, A&A, 554, A28
Cutri, R. M., Skrutskie, M. F., van Dyk, S., et al. 2003, VizieR Online Data Catalog: 2MASS All-Sky Catalog of Point Sources (Cutri+ 2003), VizieR On-line Data Catalog: II/246. Originally published in: 2003yCat.2246....0C
Cutri, R. M., Wright, E. L., Conrow, T., et al. 2021, VizieR Online Data Catalog, II/328
Dal Ponte, M., D'Orazi, V., Bragaglia, A., et al. 2025, A&A, 701, A289
Desidera, S., Sozzetti, A., Bonomo, A. S., et al. 2013, A&A, 554, A29
Dotter, A. 2016, ApJS, 222, 8
Eastman, J. D., Rodriguez, J. E., Agol, E., et al. 2019, arXiv e-prints, arXiv:1907.09480
Fitzmaurice, E., Stefánsson, G., Kavanagh, R. D., et al. 2024, AJ, 168, 140
Foreman-Mackey, D., Hogg, D. W., Lang, D., & Goodman, J. 2013, PASP, 125, 306
Gaia Collaboration. 2022, VizieR Online Data Catalog: Gaia DR3 Part 6. Performance verification (Gaia Collaboration, 2022), VizieR On-line Data Catalog: I/360. Originally published in: 2023A&A...674A...1G
Gaia Collaboration, Arenou, F., Babusiaux, C., et al. 2023a, A&A, 674, A34
Gaia Collaboration, Prusti, T., de Bruijne, J. H. J., et al. 2016, A&A, 595, A1
Gaia Collaboration, Vallenari, A., Brown, A. G. A., et al. 2023b, A&A, 674, A1
Gomes da Silva, J., Figueira, P., Santos, N., & Faria, J. 2018, The Journal of Open Source Software, 3, 667
Gomes da Silva, J., Santos, N. C., Adibekyan, V., et al. 2021, A&A, 646, A77
GRAVITY Collaboration, Abuter, R., Accardo, M., et al. 2017, A&A, 602, A94
Gustafsson, B., Edvardsson, B., Eriksson, K., et al. 2008, A&A, 486, 951
Holl, B., Sozzetti, A., Sahlmann, J., et al. 2023, A&A, 674, A10
Izidoro, A., Morbidelli, A., Raymond, S. N., Hersant, F., & Pierens, A. 2015, A&A, 582, A99
Jumper, P. H. & Fisher, R. T. 2013, ApJ, 769, 9
Kervella, P., Arenou, F., & Thévenin, F. 2022, A&A, 657, A7
Lagrange, A.-M., Meunier, N., Desort, M., & Malbet, F. 2011, A&A, 528, L9
Lanza, A. F., Molaro, P., Monaco, L., & Haywood, R. D. 2016, A&A, 587, A103
Lefèvre-Forján, E. & Mulders, G. D. 2025, ApJ, 988, 101
Lovis, C. & Pepe, F. 2007, A&A, 468, 1115
Ma, B. & Ge, J. 2014, MNRAS, 439, 2781
Mahadevan, S., Ramsey, L. W., Terrien, R., et al. 2014, in Society of Photo-Optical Instrumentation Engineers (SPIE) Conference Series, Vol. 9147, Ground-based and Airborne Instrumentation for Astronomy V, ed. S. K. Ramsay, I. S. McLean, & H. Takami, 91471G
Malavolta, L., Mayo, A. W., Louden, T., et al. 2018, AJ, 155, 107
Malavolta, L., Nascimbeni, V., Piotto, G., et al. 2016, A&A, 588, A118
Maldonado, J., Affer, L., Micela, G., et al. 2015, A&A, 577, A132
Maldonado, J., Scandariato, G., Stelzer, B., et al. 2017, A&A, 598, A27
Maldonado, J. & Villaver, E. 2017, A&A, 602, A38
Marcussen, M. L. & Albrecht, S. H. 2023, AJ, 165, 266
Marcy, G. W. & Butler, R. P. 2000, PASP, 112, 137
McQuillan, A., Mazeh, T., & Aigrain, S. 2013, ApJ, 775, L11
Meunier, N., Lagrange, A.-M., & Borgniet, S. 2020, A&A, 644, A77
Mishra, L., Alibert, Y., Udry, S., & Mordasini, C. 2023, A&A, 670, A68
Moe, M. & Di Stefano, R. 2017, ApJS, 230, 15
Morbidelli, A., Lambrechts, M., Jacobson, S., & Bitsch, B. 2015, Icarus, 258, 418
Perryman, M., Hartman, J., Bakos, G. Á., & Lindegren, L. 2014, ApJ, 797, 14
Pinamonti, M., Sozzetti, A., Barbato, D., et al. 2026, A&A, 707, A67
Pojmanski, G. 2002, Acta Astron., 52, 397
Ricker, G. R., Winn, J. N., Vanderspek, R., et al. 2015, Journal of Astronomical Telescopes, Instruments, and Systems, 1, 014003
Rosenthal, L. J., Knutson, H. A., Chachan, Y., et al. 2022, ApJS, 262, 1
Sahlmann, J., Ségransan, D., Queloz, D., et al. 2011, A&A, 525, A95
Schlecker, M., Mordasini, C., Emsenhuber, A., et al. 2021, A&A, 656, A71
Schwab, C., Rakich, A., Gong, Q., et al. 2016, in Society of Photo-Optical Instrumentation Engineers (SPIE) Conference Series, Vol. 9908, Ground-based and Airborne Instrumentation for Astronomy VI, ed. C. J. Evans, L. Simard, & H. Takami, 99087H
Sneden, C. 1973, ApJ, 184, 839
Sousa, S. G., Santos, N. C., Adibekyan, V., Delgado-Mena, E., & Israelian, G. 2015, A&A, 577, A67
Sozzetti, A. 2024, Comptes Rendus Physique, 24, 152
Sozzetti, A., Giacobbe, P., Lattanzi, M. G., et al. 2014, MNRAS, 437, 497
Sozzetti, A., Pinamonti, M., Damasso, M., et al. 2023, A&A, 677, L15
Stefánsson, G., Mahadevan, S., Winn, J. N., et al. 2025, AJ, 169, 107
Storn, R. & Price, K. 1997, Journal of Global Optimization, 11, 341
Telting, J. H., Avila, G., Buchhave, L., et al. 2014, Astronomische Nachrichten, 335, 41

Tody, D. 1993, in Astronomical Society of the Pacific Conference Series, Vol. 52, Astronomical Data Analysis Software and Systems II, ed. R. J. Hanisch, R. J. V. Brissenden, & J. Barnes, 173
Whitworth, A. 2018, arXiv e-prints, arXiv:1811.06833
Winn, J. N. 2022, AJ, 164, 196
Winterhalder, T. O., Lacour, S., Mérand, A., et al. 2024, A&A, 688, A44
Zechmeister, M. & Kürster, M. 2009, A&A, 496, 577
Zhu, W. & Wu, Y. 2018, AJ, 156, 92

---

[1] INAF – Osservatorio Astronomico di Padova, Vicolo dell'Osservatorio 5, I-35122, Padova, Italy
e-mail: domenico.barbato@inaf.it
[2] INAF – Osservatorio Astrofisico di Torino, Via Osservatorio 20, I-10025, Pino Torinese, Italy
[3] Department of Physics, University of Rome Tor Vergata, via della Ricerca Scientifica 1, I-00133, Rome, Italy
[4] INAF – Osservatorio Astronomico di Palermo, Piazza del Parlamento 1, I-90134 Palermo, Italy
[5] INAF – Osservatorio Astronomico di Roma, Via Frascati 33, I-00078, Monte Porzio Catone (Roma), Italy
[6] INAF – Osservatorio Astrofisico di Catania, Via S. Sofia 78, I-95123 Catania, Italy
[7] INAF – Osservatorio Astronomico di Trieste, via Tiepolo 11, I-34143 Trieste
[8] Dipartimento di Fisica, Università degli Studi di Torino, via P. Giuria 1, Turin, I-10125, Italy
[9] INAF – Osservatorio Astronomico di Brera, Via E. Bianchi 46, I-23807 Merate, Italy
[10] Max Planck Institute for Astronomy, Königstuhl 17, I-69117 Heidelberg, Germany
[11] Dipartimento di Fisica e Astronomia Galileo Galilei, Università degli Studi di Padova, Vicolo dell'Osservatorio 3, I-35122 Padova, Italy
[12] Centro di Ateneo di Studi e Attività Spaziali G. Colombo – Università degli Studi di Padova, Via Venezia 15, I-35131, Padova, Italy
[13] Fundacion Galileo Galilei – INAF, Rambla J.A. Fernandez P., 7, E-38712 S.C.Tenerife, Spain
[14] Instituto de Astrofísica de Canarias, C/Vía Láctea s/n, 38205 La Laguna (Tenerife), Canary Islands, Spain
[15] Departamento de Astrofísica, Univ. de La Laguna, Av. del Astrofísico Francisco Sánchez s/n, 38205 La Laguna (Tenerife), Canary Islands, Spain
[16] Dipartimento di Matematica e Fisica, Università Roma Tre, Via della Vasca Navale 84, 00146 Roma, Italy

Appendix A: Stellar and orbital parameters

Table A.1. Stellar parameters for Gaia non-single-star candidates in the sample identified as astrophysical false positives in this work.

	TYC 4338-562-1	HD 275921	TYC 4730-512-1	TYC 4106-138-1	PM J08079+2651	TYC 1546-519-1
Gaia DR3 ID	547770821740800384	230138989266819456	3205578257602278784	288196433028185728	683525873153063680	4553792062596291072
α (J2000)^a	$3^h16^m32.83^s$	$3^h56^m18.52^s$	$4^h27^m7.03^s$	$5^h54^m58.09^s$	$8^h07^m55.53^s$	$17^h29^m39.40^s$
δ (J2000)^a	+74°13′51.14″	+40°51′44.04″	-2°55′50.68″	+65°47′1.43″	+26°51′31.46″	+18°47′38.14″
ϖ (mas)^a	4.819 ± 0.015	6.082 ± 0.027	4.591 ± 0.023	7.555 ± 0.029	21.483 ± 0.032	5.150 ± 0.0160
μ_α (mas yr^{-1})^a	−5.282 ± 0.015	−22.885 ± 0.029	52.469 ± 0.022	−28.600 ± 0.019	39.641 ± 0.035	24.153 ± 0.077
μ_δ (mas yr^{-1})^a	−10.059 ± 0.018	−10.608 ± 0.031	49.380 ± 0.018	−36.909 ± 0.019	68.794 ± 0.032	26.456 ± 0.056
RUWE^a	1.50	1.54	1.42	2.10	2.63	1.47
$RV_{\rm sys}$ (km s^{-1})^a	4.12 ± 0.49	−13.72 ± 1.27	101.41 ± 0.84	3.49 ± 0.24	8.65 ± 0.01	−27.38 ± 0.43
$P_{\rm NSS}$ (d)^a	512.48 ± 7.78	739.78 ± 31.77	598.12 ± 19.31	438.23 ± 7.05	113.62 ± 0.40	988 ± 119
B (mag)^b	10.40 ± 0.03	10.77 ± 0.05	11.33 ± 0.09	12.09 ± 0.12	13.74 ± 0.05	12.06 ± 0.12
V (mag)^b	9.87 ± 0.03	10.08 ± 0.04	10.60 ± 0.07	11.16 ± 0.06	12.24 ± 0.02	11.18 ± 0.07
J (mag)^c	8.886 ± 0.030	8.934 ± 0.056	9.543 ± 0.027	9.601 ± 0.022	9.166 ± 0.021	9.863 ± 0.020
H (mag)^c	8.728 ± 0.030	8.668 ± 0.023	9.2 ± 0.026	9.139 ± 0.029	8.545 ± 0.023	9.522 ± 0.016
K (mag)^c	8.643 ± 0.022	8.593 ± 0.019	9.133 ± 0.023	9.050 ± 0.024	8.354 ± 0.017	9.462 ± 0.018
WISE1 (mag)^d	8.621 ± 0.023	8.545 ± 0.023	9.064 ± 0.022	9.015 ± 0.023	8.240 ± 0.022	9.419 ± 0.024
WISE2 (mag)^d	8.654 ± 0.019	8.571 ± 0.021	9.113 ± 0.019	9.068 ± 0.020	8.165 ± 0.020	9.465 ± 0.020
WISE3 (mag)^d	8.615 ± 0.023	8.535 ± 0.026	9.066 ± 0.029	9.027 ± 0.030	8.091 ± 0.024	9.400 ± 0.034
WISE4 (mag)^d	8.602 ± 0.412	8.010 ± 0.211	8.318 ± 0.010	8.925 ± 0.467	8.046 ± 0.251	8.995 ± 0.448
G (mag)^a	9.845 ± 0.002	9.958 ± 0.003	10.595 ± 0.003	10.951 ± 0.003	11.449 ± 0.002	11.019 ± 0.003
$G_{\rm BP}$ (mag)^a	10.110 ± 0.003	10.280 ± 0.003	10.941 ± 0.003	11.400 ± 0.003	12.468 ± 0.003	11.381 ± 0.003
$G_{\rm RP}$ (mag)^a	9.416 ± 0.004	9.466 ± 0.004	10.081 ± 0.004	10.335 ± 0.004	10.452 ± 0.004	10.486 ± 0.004
Spectral Type	F8	G5	G6	K0	K7	K0
$M_\star$ ($M_\odot$)^e	$1.46^{+0.13}_{-0.14}$	$1.18^{+0.13}_{-0.15}$	$1.20^{+0.17}_{-0.18}$	$0.960^{+0.072}_{-0.064}$	0.641 ± 0.027	$1.030^{+0.096}_{-0.097}$
$R_\star$ ($R_\odot$)^e	$1.667^{+0.085}_{-0.077}$	$1.374^{+0.065}_{-0.062}$	$1.64^{+0.13}_{-0.12}$	$0.987^{+0.043}_{-0.038}$	$0.622^{+0.021}_{-0.020}$	$1.127^{+0.050}_{-0.047}$
$\rho_\star$ (g cm^{-3})^e	$0.442^{+0.087}_{-0.080}$	$0.64^{+0.13}_{-0.12}$	$0.384^{+0.11}_{-0.093}$	$1.41^{+0.20}_{-0.18}$	$3.76^{+0.33}_{-0.31}$	$1.01^{+0.17}_{-0.15}$
$L_\star$ ($L_\odot$)^e	$5.4^{+1.4}_{-1.0}$	$2.62^{+0.56}_{-0.40}$	$3.28^{+0.88}_{-0.66}$	$0.873^{+0.11}_{-0.100}$	$0.0810^{+0.0069}_{-0.0059}$	$1.41^{+0.22}_{-0.18}$
Age (Gyr)^e	$1.41^{+1.3}_{-0.88}$	$3.5^{+3.9}_{-2.4}$	$4.4^{+4.1}_{-2.4}$	$6.4^{+4.5}_{-4.1}$	$7.4^{+4.4}_{-4.8}$	$5.4^{+4.6}_{-3.5}$
$T_{\rm eff}$ (K)^e	6800^{+440}_{-400}	6270^{+340}_{-290}	6090^{+350}_{-340}	5610^{+150}_{-140}	3907^{+58}_{-56}	5930^{+220}_{-210}
log g (cgs)^e	$4.157^{+0.061}_{-0.069}$	$4.234^{+0.064}_{-0.080}$	$4.090^{+0.083}_{-0.098}$	4.431 ± 0.045	$4.657^{+0.024}_{-0.025}$	$4.347^{+0.053}_{-0.058}$
[Fe/H]^e	$-0.05^{+0.25}_{-0.30}$	$-0.09^{+0.20}_{-0.25}$	$-0.10^{+0.27}_{-0.28}$	$0.07^{+0.18}_{-0.16}$	$0.31^{+0.12}_{-0.15}$	$-0.02^{+0.21}_{-0.23}$

Notes. $^{(a)}$ retrieved from Gaia Data Release 3 (Gaia Collaboration et al. 2023b) $^{(b)}$ retrieved from Chambers et al. (2016) $^{(c)}$ retrieved from Cutri et al. (2003) $^{(d)}$ retrieved from Cutri et al. (2021) $^{(e)}$ obtained from the SED fitting discussed in Sect. 2

Table A.2. Stellar parameters for Gaia non-single-star candidates in the sample validated and confirmed in this work.

	2MASS J20570943+1406590	HIP 105707	TYC 198-493-1	HIP 60865	PM J13580+3141	TYC 3456-251-1	TYC 4998-437-1	StKM 1-1494
Gaia DR3 ID	1761619456801656064	1853704144046204032	3087990814774129920	1518957932040718464	1457486023639239296	1543883104727682176	6330529666839726592	4169462136799175296
α (J2000)[a]	$20^h57^m9.44^s$	$21^h24^m36.60^s$	$8^h2^m5.21^s$	$12^h28^m30.86^s$	$13^h58^m01.62^s$	$12^h33^m40.86^s$	$14^h46^m31.25^s$	$17^h34^m46.72^s$
δ (J2000)[a]	+14°06′59.03″	+32°07′22.76″	+2°36′44.63″	+35°16′36.79″	+31°41′43.48″	+48°38′39.28″	-7°24′34.41″	-06°54′10.72″
ϖ (mas)[a]	9.080 ± 0.019	19.871 ± 0.023	13.297 ± 0.035	13.395 ± 0.026	13.643 ± 0.025	6.485 ± 0.024	7.673 ± 0.041	35.793 ± 0.024
μ_α (mas yr^{-1})[a]	19.517 ± 0.022	−156.591 ± 0.034	−35.016 ± 0.041	−278.109 ± 0.023	−75.528 ± 0.023	−36.293 ± 0.019	−94.926 ± 0.036	−8.747 ± 0.034
μ_δ (mas yr^{-1})[a]	−47.591 ± 0.017	−116.689 ± 0.023	−21.455 ± 0.021	2.888 ± 0.024	18.101 ± 0.017	−12.127 ± 0.022	34.270 ± 0.031	−74.531 ± 0.025
U (km s^{-1})[b]	−11.055 ± 0.199	−43.670 ± 0.075	13.371 ± 0.291	83.461 ± 0.176	26.053 ± 0.043	12.884 ± 0.171	79.715 ± 1.092	−1.193 ± 0.454
V (km s^{-1})[b]	−9.049 ± 0.364	−17.177 ± 0.297	−12.025 ± 0.234	−49.466 ± 0.100	−15.547 ± 0.023	−27.470 ± 0.196	−14.497 ± 0.294	−9.191 ± 0.145
W (km s^{-1})[b]	−23.381 ± 0.156	9.698 ± 0.0.070	−9.813 ± 0.120	−20.128 ± 0.405	−10.428 ± 0.014	−20.694 ± 0.594	−0.159 ± 1.139	−4.467 ± 0.115
RUWE[a]	1.97	2.819	3.26	3.84	1.16	2.68	1.63	3.15
RV_{sys} (km s^{-1})[a]	5.4402 ± 0.4397	−11.21 ± 0.31	14.33 ± 0.39	−11.3957 ± 0.4102	−17.348 ± 0.008	−23.80 ± 0.64	−51.74 ± 1.57	−2.66 ± 0.49
B (mag)[c]	13.23 ± 0.03	12.66 ± 0.17	11.33 ± 0.11	14.16 ± 0.49	13.82 ± 0.02	12.56 ± 0.16	12.15 ± 0.26	12.80 ± 0.28
V (mag)[c]	12.26 ± 0.05	11.20 ± 0.06	10.58 ± 0.08	12.256 ± 0.20	12.52 ± 0.02	11.76 ± 0.11	11.31 ± 0.15	11.24 ± 0.01
J (mag)[d]	10.27 ± 0.02	8.75 ± 0.02	8.91 ± 0.02	9.75 ± 0.02	9.94 ± 0.02	10.23 ± 0.02	10.03 ± 0.02	8.30 ± 0.02
H (mag)[d]	9.65 ± 0.03	8.11 ± 0.02	8.49 ± 0.03	9.12 ± 0.04	9.30 ± 0.01	9.86 ± 0.02	9.58 ± 0.02	7.71 ± 0.03
K (mag)[d]	9.59 ± 0.01	7.98 ± 0.02	8.41 ± 0.02	9.01 ± 0.02	9.13 ± 0.02	9.79 ± 0.02	9.52 ± 0.02	7.45 ± 0.027
WISE1 (mag)[e]	9.52 ± 0.02	7.91 ± 0.02	8.37 ± 0.02	8.92 ± 0.02	9.05 ± 0.02	9.76 ± 0.02	9.44 ± 0.02	7.34 ± 0.03
WISE2 (mag)[e]	9.59 ± 0.02	7.99 ± 0.02	8.41 ± 0.02	8.97 ± 0.02	9.11 ± 0.02	9.80 ± 0.02	9.495 ± 0.02	7.34 ± 0.02
WISE3 (mag)[e]	9.49 ± 0.03	7.89 ± 0.02	8.36 ± 0.02	8.89 ± 0.03	8.99 ± 0.03	9.75 ± 0.04	9.411 ± 0.03	7.27 ± 0.02
WISE4 (mag)[e]	8.44 ± 0.02	7.64 ± 0.13	8.50 ± 0.38	8.71 ± 0.38	8.86 ± 0.35	8.53 ± 0.01	8.817 ± 0.03	7.16 ± 0.10
G (mag)[a]	11.88 ± 0.02	10.568 ± 0.003	10.162 ± 0.003	11.622 ± 0.003	11.909 ± 0.003	11.401 ± 0.003	11.421 ± 0.003	10.535 ± 0.003
G_{BP} (mag)[a]	12.46 ± 0.02	11.298 ± 0.003	10.588 ± 0.003	12.361 ± 0.003	12.723 ± 0.003	11.779 ± 0.003	11.893 ± 0.003	11.520 ± 0.003
G_{RP} (mag)[a]	11.15 ± 0.02	9.740 ± 0.004	9.571 ± 0.003	10.784 ± 0.004	11.025 ± 0.004	10.854 ± 0.004	10.787 ± 0.04	9.553 ± 0.003
Spectral Type	K4	K6/K7	K0	K7	K7	G9	K1	M0
T_{eff} (K)[f]	4590 ± 75	4201 ± 45	5250 ± 90	4142 ± 45	4088 ± 45	5400 ± 150	5150 ± 100	3855 ± 45
log g (cgs)[f]	4.50 ± 0.11	4.66 ± 0.02	4.58 ± 0.25	4.66 ± 0.02	4.66 ± 0.02	4.25 ± 0.35	4.40 ± 0.30	4.68 ± 0.02
[Fe/H][f]	−0.27 ± 0.07	0.01 ± 0.11	−0.06 ± 0.05	0.02 ± 0.11	0.01 ± 0.11	−0.18 ± 0.05	0.01 ± 0.05	−0.01 ± 0.11
v_{micro} (km s^{-1})[f]	0.80 ± 0.05	–	0.30 ± 0.15	–	–	0.80 ± 0.15	0.35 ± 0.10	–
$M_\star$ ($M_\odot$)[g]	$0.689^{+0.031}_{-0.030}$	$0.707^{+0.028}_{-0.026}$	$0.817^{+0.037}_{-0.035}$	0.683 ± 0.026	$0.652^{+0.027}_{-0.025}$	$0.854^{+0.050}_{-0.041}$	$0.856^{+0.043}_{-0.035}$	0.584 ± 0.027
$R_\star$ ($R_\odot$)[g]	$0.687^{+0.033}_{-0.030}$	$0.710^{+0.018}_{-0.017}$	$0.774^{+0.026}_{-0.023}$	$0.679^{+0.018}_{-0.017}$	$0.641^{+0.020}_{-0.018}$	$0.879^{+0.069}_{-0.059}$	$0.871^{+0.050}_{-0.046}$	0.571 ± 0.022
$\rho_\star$ (g cm^{-3})[g]	$3.00^{+0.38}_{-0.35}$	$2.78^{+0.20}_{-0.19}$	$2.49^{+0.24}_{-0.23}$	$3.08^{+0.23}_{-0.22}$	$3.48^{+0.28}_{-0.27}$	$1.78^{+0.38}_{-0.34}$	$1.83^{+0.30}_{-0.26}$	$4.43^{+0.44}_{-0.41}$
$L_\star$ ($L_\odot$)[g]	$0.197^{+0.022}_{-0.018}$	$0.148^{+0.007}_{-0.006}$	$0.406^{+0.036}_{-0.029}$	$0.127^{+0.007}_{-0.005}$	$0.106^{+0.007}_{-0.006}$	$0.63^{+0.13}_{-0.10}$	$0.502^{+0.074}_{-0.065}$	$0.067^{+0.006}_{-0.005}$
Age_{SED} (Gyr)[g]	$7.8^{+4.3}_{-6.4}$	$9.2^{+3.3}_{-5.1}$	$5.3^{+4.8}_{-3.6}$	$8.5^{+3.7}_{-4.9}$	$7.7^{+4.2}_{-4.8}$	$8.2^{+3.9}_{-4.7}$	$9.1^{+3.3}_{-4.9}$	$7.4^{+4.5}_{-4.9}$
Age_{kin} (Gyr)[b]	~ 2.37	~ 4.92	~ 0.556	~ 10.72	~ 0.77	~ 2.31	~ 5.42	~ 0.60
S_{MW}[h]	0.166 ± 0.034	0.386 ± 0.034	0.195 ± 0.035	0.348 ± 0.052	0.837 ± 0.050	0.150 ± 0.012	0.097 ± 0.019	1.183 ± 0.091
Hα[h]	0.165 ± 0.008	0.223 ± 0.006	0.207 ± 0.006	0.225 ± 0.013	0.350 ± 0.011	0.260 ± 0.007	0.447 ± 0.012	0.328 ± 0.016
Na I[h]	0.315 ± 0.024	0.299 ± 0.010	0.832 ± 0.025	0.323 ± 0.028	0.425 ± 0.018	1.286 ± 0.066	1.221 ± 0.057	0.312 ± 0.011
He I[h]	0.557 ± 0.005	0.580 ± 0.003	0.551 ± 0.003	0.574 ± 0.003	0.574 ± 0.002	0.546 ± 0.003	0.552 ± 0.006	0.569 ± 0.003

Notes. [(a)] retrieved from Gaia Data Release 3 (Gaia Collaboration et al. 2023b; Gaia Collaboration 2022) [(b)] obtained from the proper motion analysis discussed in Sect 2 [(c)] retrieved from Chambers et al. (2016) [(d)] retrieved from Cutri et al. (2003) [(e)] retrieved from Cutri et al. (2021) [(f)] obtained from spectroscopical analysis discussed in Sect. 2 [(g)] obtained from the SED fitting discussed in Sect. 2 [(h)] obtained from activity analysis discussed in Sect. 2

Table A.3. HARPS-N observational statistics, selected Gaia DR3 NSS astrometric candidate solution parameters and RV best-fit orbital solutions for the companions detected in this work.

	2MASS J20570943+1406590	HIP 105707	TYC 198-493-1	HIP 60865	PM J13580+3141	TYC 3456-251-1	TYC 4998-437-1	StKM 1-1494
Observation start	10/2023	10/2023	11/2023	12/2023	01/2024	12/2023	04/2024	04/2024
Observation end	12/2024	11/2025	01/2026	04/2025	07/2025	06/2025	07/2025	09/2025
$N_{\rm RV}$	31	59	33	22	17	28	16	35
$t_{\rm span}$ (d)	428	785	796	499	547	538	446	519
$P_{\rm cov}$ (%)	150	114	110	99	96	90	85	62
$\overline{\sigma}_{\rm RV}$ (m s^{-1})	2.38	1.36	1.45	2.28	2.95	2.46	1.97	1.93
w.r.m.s. (m s^{-1})	544	344	173	999	275	1187	459	1318
$P_{\rm NSS}$ (d)	280.76 ± 3.16	687.71 ± 12.67	722.60 ± 8.79	500.69 ± 4.88	564.02 ± 11.19	592.66 ± 7.89	526.14 ± 23.10	829.40 ± 1.76
$e_{\rm NSS}$	0.33 ± 0.13	0.51 ± 0.03	0.75 ± 0.07	0.25 ± 0.06	0.51 ± 0.19	0.14 ± 0.07	0.43 ± 0.16	0.328 ± 0.006
$i_{\rm NSS}$ (deg)	57.15 ± 4.37	124.06 ± 2.08	14.62 ± 18.02	82.73 ± 1.77	115.43 ± 4.60	62.57 ± 3.68	127.69 ± 10.62	93.80 ± 0.34
$\omega_{\rm NSS}$ (deg)	249.81 ± 16.18	199.57 ± 5.01	321.49 ± 78.48	103.41 ± 12.72	185.92 ± 16.18	51.91 ± 30.56	185.69 ± 22.78	92.95 ± 1.58
lower $M_{\rm NSS}$ ($M_{\rm Jup}$)	38.78	23.77	49	46.97	11.66	52.3	33.61	64.2
$a_{0,\rm NSS}$ (mas)	0.37 ± 0.02	0.91 ± 0.02	1.22 ± 0.14	0.98 ± 0.03	0.31 ± 0.04	0.50 ± 0.02	0.40 ± 0.05	5.38 ± 0.02
$K_{\rm NSS}$ (m s^{-1})	1405.20 ± 124.07.	697.73 ± 30.04	527.12 ± 641.58.	1628.60 ± 58.89	460.15 ± 86.89	1268.67 ± 69.51	944.79 ± 200.90	2082.44 ± 10.16
$P_{\rm b}$ (d)	281.89 ± 0.09	$668.76^{+2.54}_{-2.60}$	$718.67^{+6.41}_{-6.35}$	528.08 ± 0.39	$588.58^{+2.15}_{-2.50}$	$592.66^{+4.92}_{-4.31}$	$558.67^{+2.80}_{-2.47}$	$789.26^{+10.08}_{-11.25}$
$K_{\rm b}$ (m s^{-1})	$1233.31^{+3.99}_{-3.91}$	$707.60^{+7.78}_{-7.15}$	$335.09^{+4.21}_{-3.89}$	$1418.62^{+1.81}_{-1.76}$	$347.42^{+2.15}_{-2.75}$	$1662.35^{+17.60}_{-15.22}$	$738.92^{+1.75}_{-1.87}$	$1984.95^{+11.16}_{-18.19}$
λ_0 (deg)	$158.51^{+0.41}_{-0.40}$	$-54.31^{+2.91}_{-2.99}$	$152.79^{+5.66}_{-6.05}$	$289.47^{+0.52}_{-0.54}$	$452.61^{+4.71}_{-5.31}$	$106.19^{+4.67}_{-4.21}$	$425.03^{+4.08}_{-3.63}$	$292.45^{+7.20}_{-8.48}$
$\sqrt{e_{\rm b}}\sin\omega_{\rm b}$	−0.558 ± 0.002	−0.260 ± 0.005	0.838 ± 0.005	0.448 ± 0.002	−0.197 ± 0.26	−0.547 ± 0.003	0.341 ± 0.004	−0.575 ± 0.006
$\sqrt{e_{\rm b}}\cos\omega_{\rm b}$	0.040 ± 0.002	−0.704 ± 0.002	$0.192^{+0.027}_{-0.029}$	−0.245 ± 0.002	$-0.528^{0.015}_{-0.013}$	−0.296 ± 0.005	−0.664 ± 0.002	$0.060^{+0.006}_{-0.005}$
$e_{\rm b}$	0.313 ± 0.002	0.563 ± 0.005	0.739 ± 0.006	0.261 ± 0.002	$0.318^{+0.011}_{-0.012}$	0.387 ± 0.003	0.557 ± 0.002	0.335 ± 0.007
$\omega_{\rm b}$ (deg)	$-85.94^{+0.22}_{-0.23}$	$-159.72^{+0.39}_{-0.37}$	$77.10^{+1.98}_{-1.84}$	118.68 ± 0.28	$-159.52^{+2.83}_{-2.84}$	$-118.43^{+0.51}_{-0.49}$	152.81 ± 0.32	$-84.06^{+0.60}_{-0.51}$
$M_{\rm b}\sin i$ ($M_{\rm Jup}$)	$30.32^{+0.84}_{-0.91}$	20.34 ± 0.58	8.63 ± 2.52	43.93 ± 1.09	10.30 ± 0.45	$59.52^{+2.46}_{-2.38}$	$22.80^{+0.75}_{-0.77}$	$63.35^{+1.93}_{-2.03}$
$a_{\rm b}$ (au)	0.75 ± 0.01	1.34 ± 0.02	$1.47^{+0.19}_{-0.23}$	1.15 ± 0.01	1.20 ± 0.02	1.34 ± 0.03	1.27 ± 0.02	1.44 ± 0.02
$M_{b,i_{\rm NSS}}$ ($M_{\rm Jup}$)	$36.09^{+2.34}_{-2.38}$	$24.55^{+1.01}_{-1.01}$	34.19 ± 21.72	44.29 ± 1.11	11.41 ± 0.69	$67.06^{+3.75}_{-3.68}$	28.81 ± 5.30	$63.49^{+1.93}_{-2.03}$
$\gamma_{\rm HARPS-N}$ (m s^{-1})	$-510.58^{+1.76}_{-1.70}$	$-280.73^{+5.87}_{-6.22}$	$-118.56^{+2.19}_{-2.24}$	$-706.32^{+1.15}_{-1.13}$	$212.90^{+8.04}_{-7.33}$	$137.47^{+16.10}_{-18.61}$	$246.62^{+0.98}_{-0.89}$	$-621.60^{+16.97}_{-25.95}$
$\dot{j}_{\rm HARPS-N}$ (m s^{-1})	$1.63^{+0.75}_{-0.78}$	$3.78^{+0.46}_{-0.40}$	$9.19^{+1.70}_{-1.35}$	$2.98^{+1.06}_{-0.86}$	$8.29^{+2.62}_{-1.83}$	$12.19^{+2.21}_{-1.73}$	$1.91^{+1.08}_{-0.89}$	$6.80^{+1.18}_{-0.98}$
$\gamma_{\rm HPF}$ (m s^{-1})	–	–	–	–	$-53.67^{+7.84}_{-7.57}$	–	–	–
$\dot{j}_{\rm HPF}$ (m s^{-1})	–	–	–	–	$15.12^{+10.14}_{-7.65}$	–	–	–
$\gamma_{\rm NEID}$ (m s^{-1})	–	–	–	–	$-33.52^{+11.07}_{-10.61}$	–	–	–
$\dot{j}_{\rm NEID}$ (m s^{-1})	–	–	–	–	$19.57^{+9.49}_{-6.16}$	–	–	–
$\gamma_{\rm FIES}$ (m s^{-1})	–	–	–	–	$61.13^{+10.05}_{-9.94}$	–	–	–
$\dot{j}_{\rm FIES}$ (m s^{-1})	–	–	–	–	$10.40^{+14.83}_{-7.25}$	–	–	–

Appendix B: Radial velocity and activity timeseries

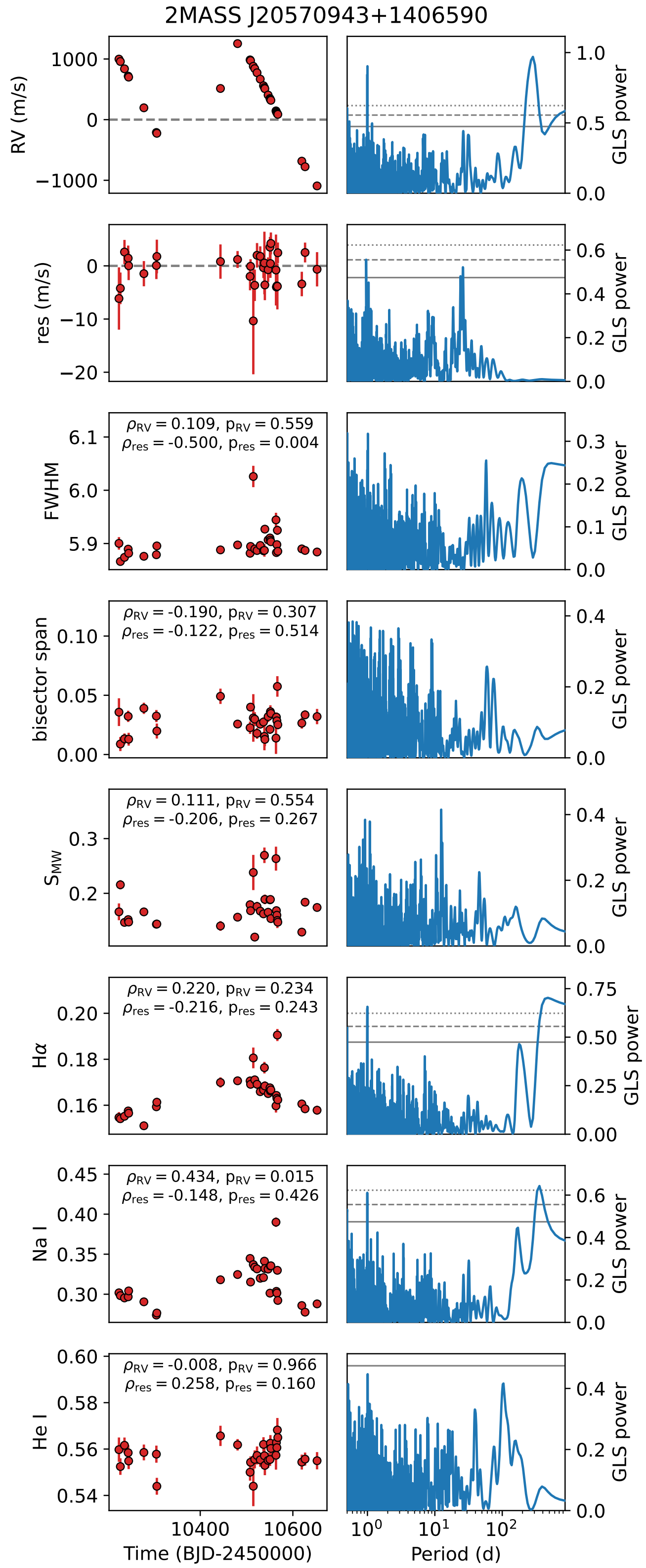

Fig. B.1. *Left panels*: time series for the HARPS-N median-subtracted radial velocity data of 2MASS J20570943+1406590, post-Keplerian fit residuals and activity indices. For the activity indices time series, the Pearson correlation coefficient and its p-value with both original and residual RVs are noted. *Right panels*: corresponding generalised Lomb-Scargle periodograms of the time series, with horizontal solid, dashed and dotted lines marking the 10%, 1% and 0.1% FAP thresholds.

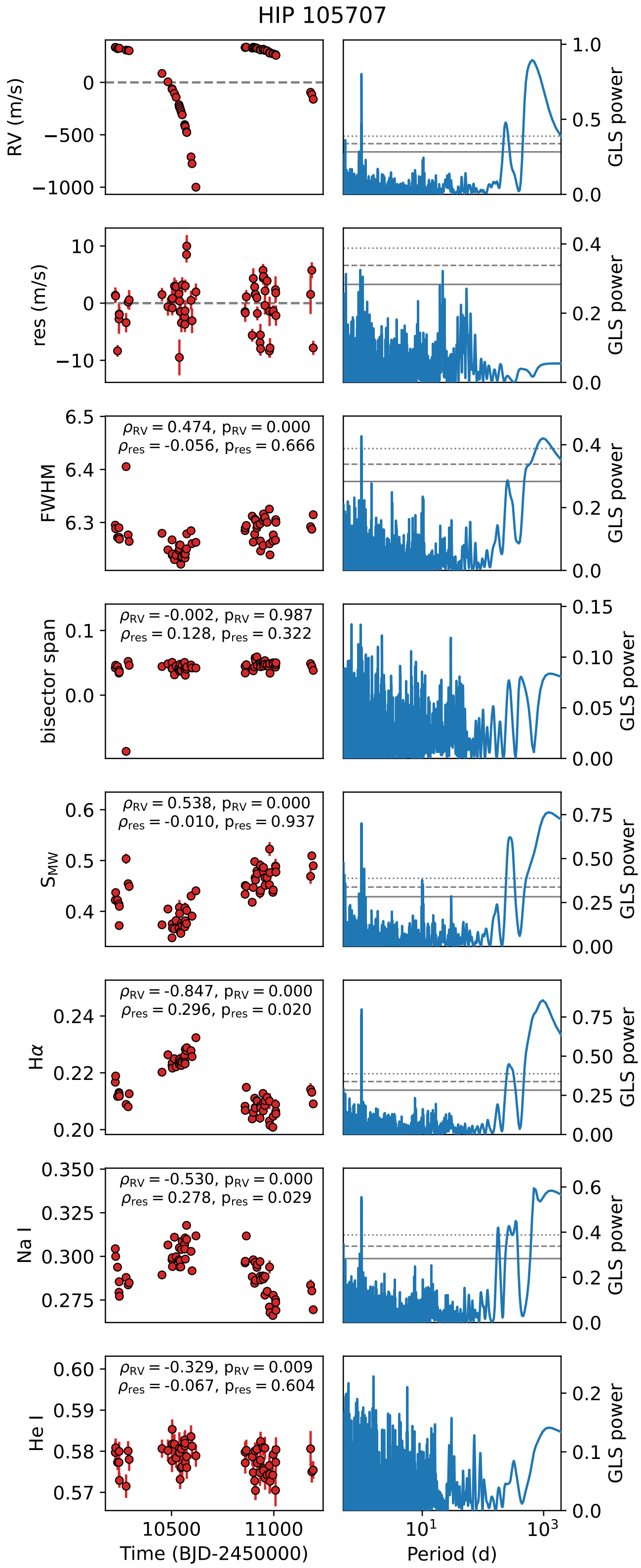

Fig. B.2. Same as Fig. B.1 but for star HIP 105707

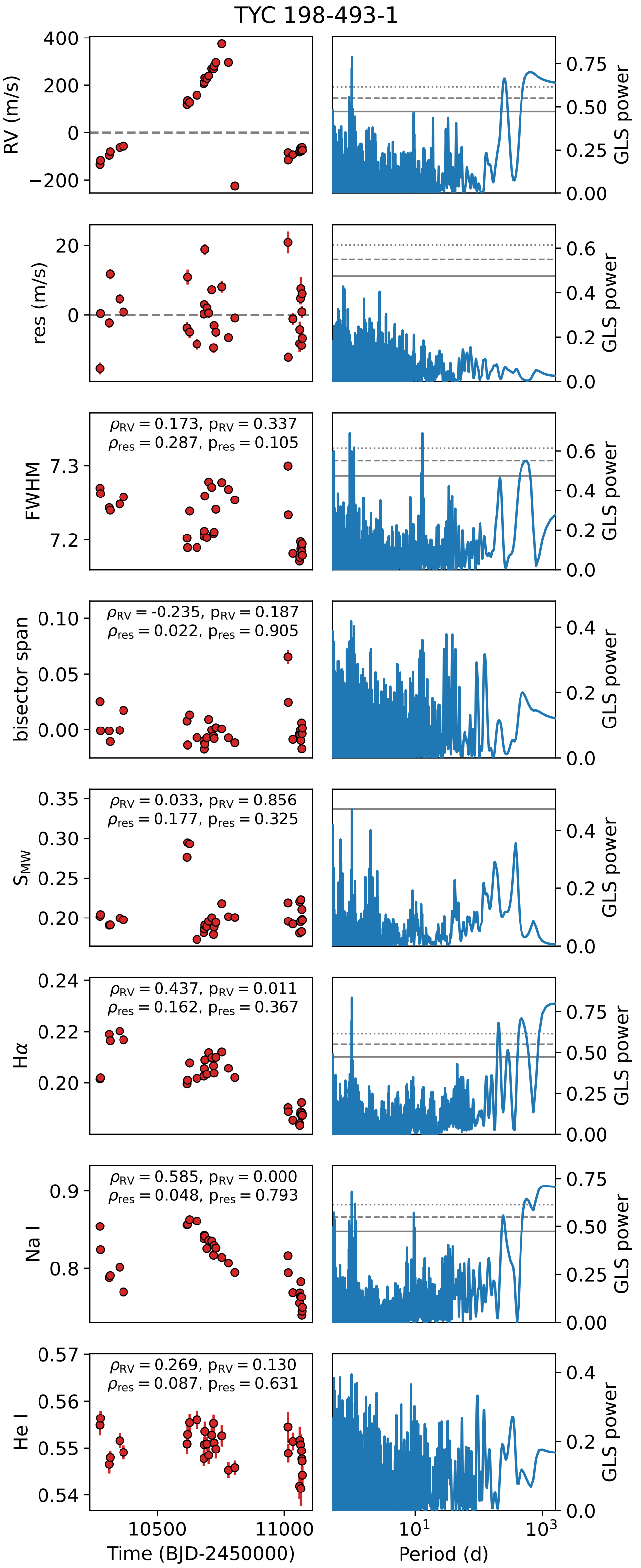

Fig. B.3. Same as Fig. B.1 but for star TYC 198-493-1

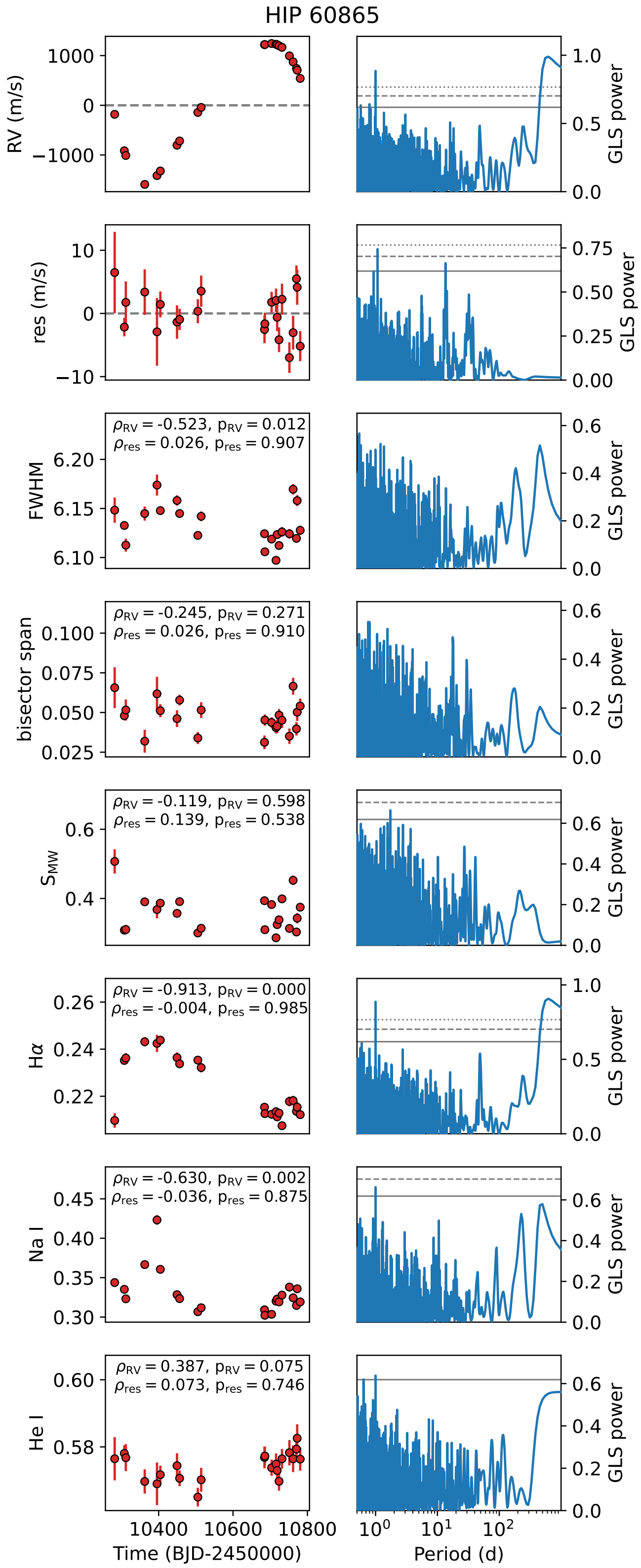

Fig. B.4. Same as Fig. B.1 but for star HIP 60865

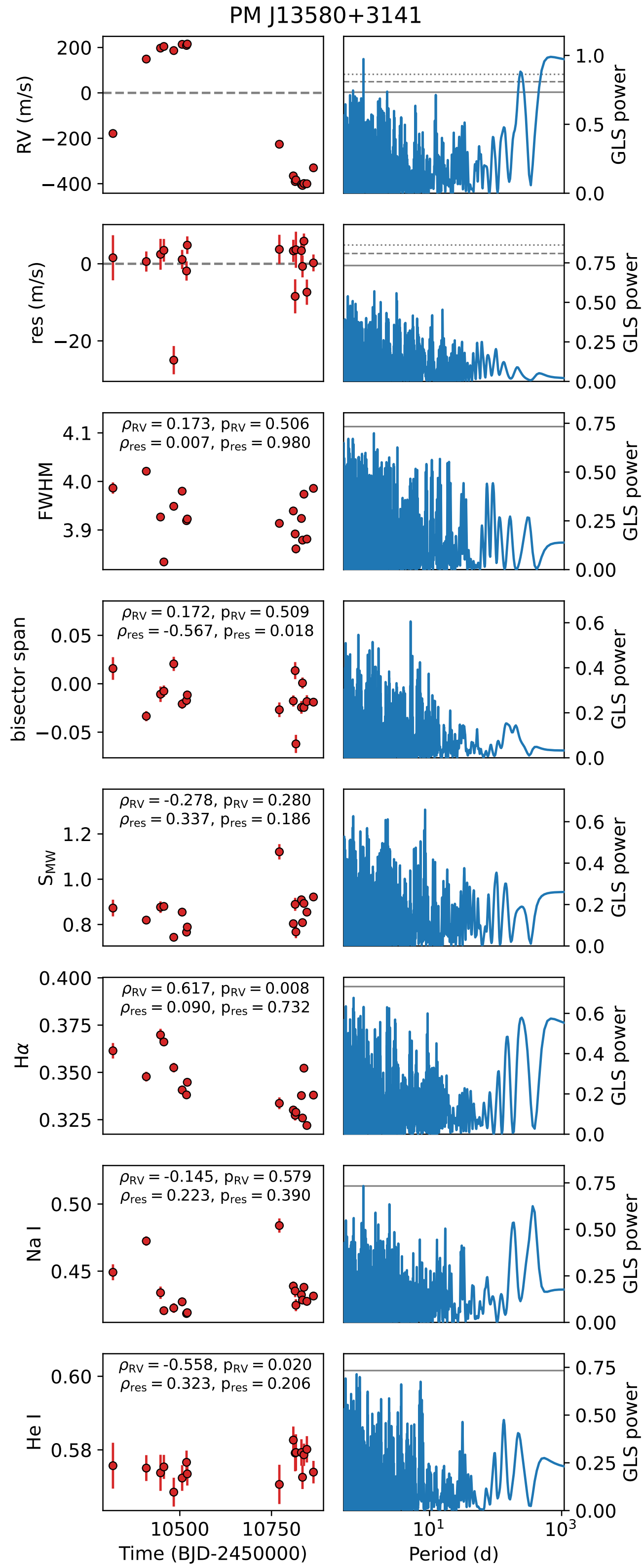

Fig. B.5. Same as Fig. B.1 but for star PM J13580+3141

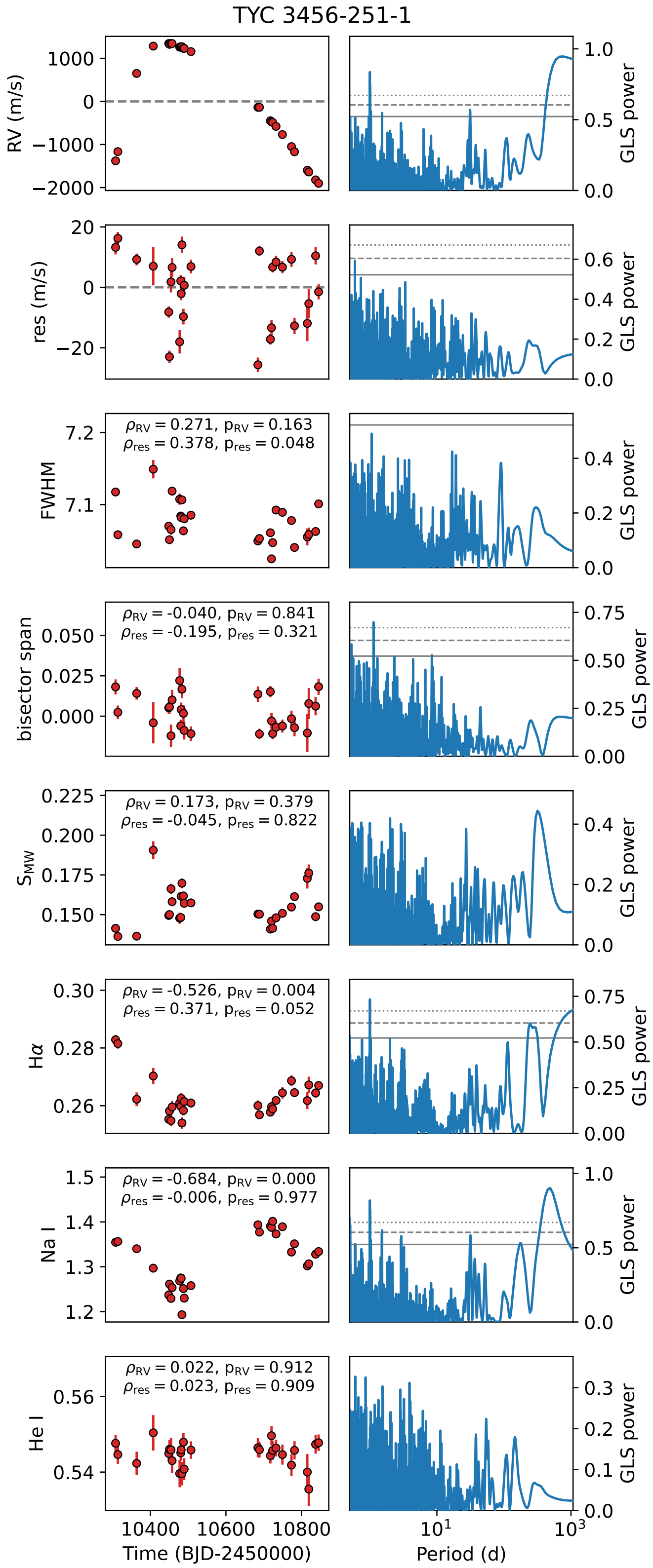

Fig. B.6. Same as Fig. B.1 but for star TYC 3456-251-1

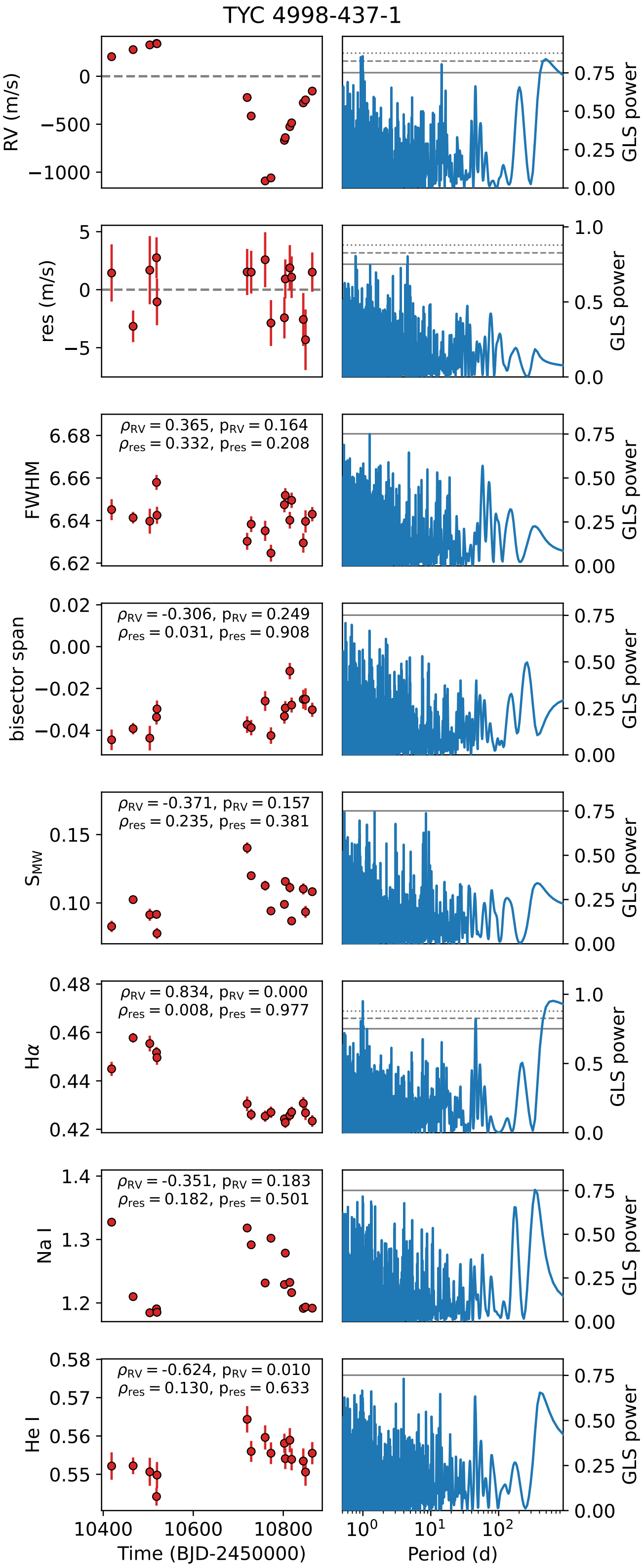

Fig. B.7. Same as Fig. B.1 but for star TYC 4998-437-1

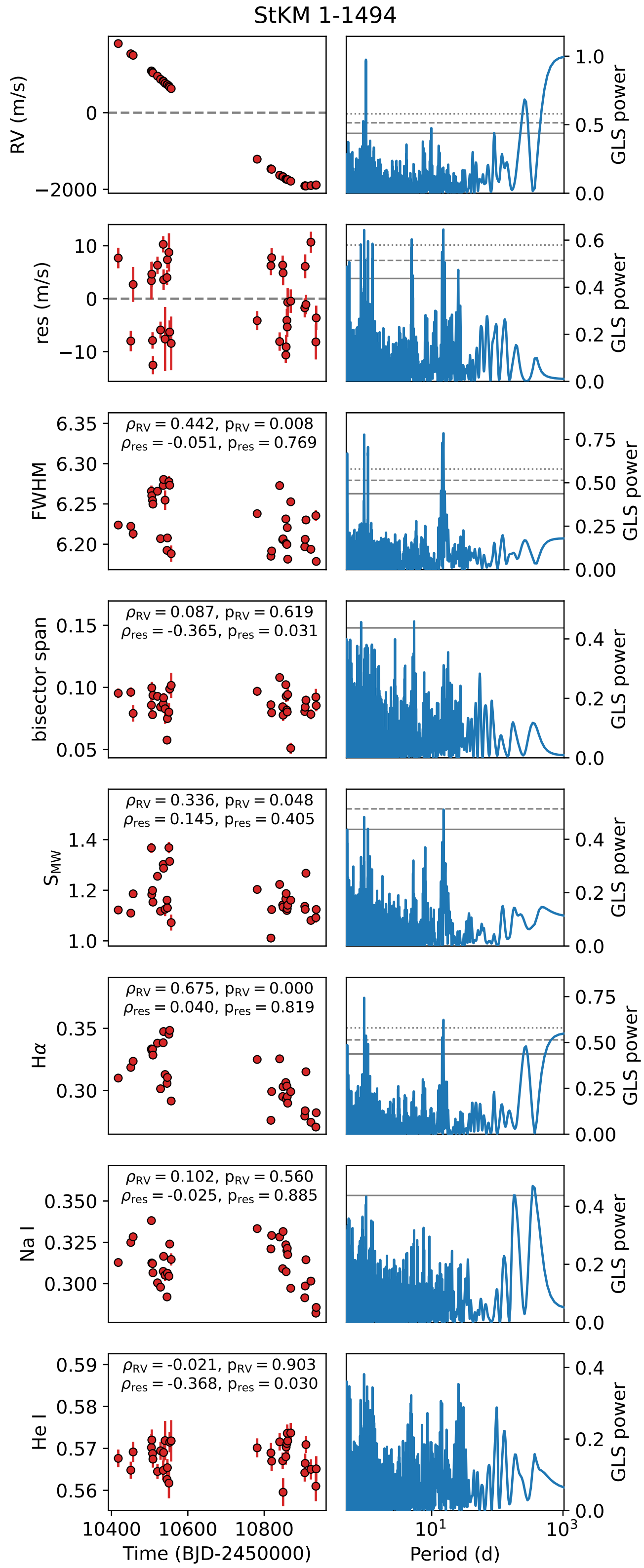

Fig. B.8. Same as Fig. B.1 but for star StKM 1-1494